AGU PUBLICATIONS

JGR

Journal of Geophysical Research: Space Physics

RESEARCH ARTICLE
10.1002/2016JA023625

Key Points:
- Substorm occurrence rates and substorm recurrence times are studied and compared with the properties of the time-varying solar wind at Earth
- The mesoscale structure of the solar wind magnetic field plays a role in the occurrence statistics of substorms
- The period of periodic substorms may be a combination of an intrinsic magnetospheric period plus variations of the solar wind magnetic field

Supporting Information:
- Text S1
- Text S2
- Text S3

Correspondence to:
J. E. Borovsky,
jborovsky@spacescience.org

Citation:
Borovsky, J. E., and K. Yakymenko (2017), Substorm occurrence rates, substorm recurrence times, and solar wind structure, *J. Geophys. Res. Space Physics*, *122*, 2973-2998, doi:10.1002/2016JA023625.

Received 24 OCT 2016
Accepted 16 FEB 2017
Accepted article online 20 FEB 2017
Published online 7 MAR 2017

Substorm occurrence rates, substorm recurrence times, and solar wind structure

Joseph E. Borovsky[1,2] **and Kateryna Yakymenko**[3,4]

[1]Space Science Institute, Boulder, Colorado, USA, [2]CSSE, University of Michigan, Ann Arbor, Michigan, USA, [3]Department of Physics and Engineering Physics, University of Saskatchewan, Saskatoon, Saskatchewan, Canada, [4]Space Weather Summer School, Los Alamos National Laboratory, Los Alamos, New Mexico, USA

Abstract Two collections of substorms are created: 28,464 substorms identified with jumps in the SuperMAG *AL* index in the years 1979–2015 and 16,025 substorms identified with electron injections into geosynchronous orbit in the years 1989–2007. Substorm occurrence rates and substorm recurrence-time distributions are examined as functions of the phase of the solar cycle, the season of the year, the Russell-McPherron favorability, the type of solar wind plasma at Earth, the geomagnetic-activity level, and as functions of various solar and solar wind properties. Three populations of substorm occurrences are seen: (1) quasiperiodically occurring substorms with recurrence times (waiting times) of 2–4 h, (2) randomly occurring substorms with recurrence times of about 6–15 h, and (3) long intervals wherein no substorms occur. A working model is suggested wherein (1) the period of periodic substorms is set by the magnetosphere with variations in the actual recurrence times caused by the need for a solar wind driving interval to occur, (2) the mesoscale structure of the solar wind magnetic field triggers the occurrence of the random substorms, and (3) the large-scale structure of the solar wind plasma is responsible for the long intervals wherein no substorms occur. Statistically, the recurrence period of periodically occurring substorms is slightly shorter when the ram pressure of the solar wind is high, when the magnetic field strength of the solar wind is strong, when the Mach number of the solar wind is low, and when the polar-cap potential saturation parameter is high.

1. Introduction

The analysis of the waiting times (recurrence times) Δt between the occurrence of "subsequent" substorm onsets (with the onsets determined by ion and electron injections into geosynchronous orbit) found indications that substorms occur in two fashions, with distinct populations of randomly occurring substorms and periodically occurring substorms [*Borovsky et al.*, 1993]. Information-theoretic statistics were used to examine the recurrence times Δt between substorm onsets (with the onsets determined by particle injections and by jumps in the *AL* index) to verify that substorms do occur in a periodic fashion with a period of 2–4 h [*Prichard et al.*, 1996]. It was speculated [*Borovsky et al.*, 1993; *Belian et al.*, 1994] that randomly occurring substorms are associated with randomly occurring intervals of enhanced solar wind driving of the magnetosphere and that periodic substorms occur during time intervals when the solar wind driving of the magnetosphere is quasi-continuous.

Substorms and substorm occurrence rates are important to understand. A substorm results in a morphological transition of the magnetosphere, changing the magnetic field configuration of the near-Earth magnetotail [*McPherron et al.*, 1973] and ejecting a portion of the magnetotail and its plasma downtail [*Hones*, 1977]. A substorm produces a substantial energy transfer from the magnetotail to the ionosphere [*Baumjohann and Kamide*, 1984] and to magnetospheric plasma populations [*Baumjohann et al.*, 1991]. Substorm occurrence is important for the evolution of the outer electron radiation belt: (1) substorm-injected electrons are probably the seed population for the radiation belt [*McDiarmid and Burrows*, 1965; *Friedel et al.*, 2002], (2) plasma waves in the dipolar magnetosphere that are driven by the injected-particle populations may resonantly energize radiation-belt electrons to relativistic energies [*Meredith et al.*, 2001; *He et al.*, 2015], and (3) the induction electric fields of repeated substorms may directly energize radiation-belt electrons as the electrons drift across the nightside of the dipole during substorm expansion phases [*Kim et al.*, 2000; *Fok et al.*, 2001; *Dai et al.*, 2014]. Under special circumstances substorms can also directly produce MeV electrons and protons [*Ingraham et al.*, 2001; *Borovsky et al.*, 2016]. Substorm injections may also produce ULF waves in the dipolar magnetosphere [*Southwood*, 1976; *Anderson et al.*, 1990; *Zolotukhina et al.*, 2008], and substorm injections

have been suspected to produce outward transport of the plasmasphere [*Spiro et al.*, 1981; *Borovsky et al.*, 2014]. Among the population of periodically occurring substorms, a subset of "global sawtooth oscillations" was found [cf. *Borovsky*, 2004; *Henderson*, 2004; *Henderson et al.*, 2006a, 2006b; *Cai et al.*, 2006, 2011]. Whereas typical substorms involve a stretching and sudden dipolarization of the nightside magnetic field, global sawtooth oscillations involve sudden morphological changes in the dayside magnetosphere (as well as the nightside magnetosphere) and sudden changes in dayside currents. In the present study, global sawtooth oscillations will not be separated from periodic substorms.

Two outstanding questions about the occurrence of substorms are the following. (1) What in the solar wind gives rise to the occurrence of random magnetospheric substorms and of periodic magnetospheric substorms? (2) What determines the magnetosphere's ~3 h periodicity for the recurrence of substorms?

In general, the substorm occurrence rate is not well known, particularly the rate versus the strength of the solar wind driving, the rate versus the type of solar wind plasma, the rate through the phases of the solar cycle, or the rate in the various phases of the different types of geomagnetic storms. Substorms are known to be associated with intervals of southward interplanetary magnetic field (IMF) [*Fairfield and Cahill*, 1966; *Caan et al.*, 1978; *Morley and Freeman*, 2007; *Wild et al.*, 2009; *Newell and Liou*, 2011]. Studies of the occurrence rates of substorms are limited to studies of the rates as functions of the solar cycle [*Borovsky and Nemzek*, 1994; *Nevanlinna and Pulkkinen*, 1998; *Tanskanen*, 2009; *Tanskanen et al.*, 2011; *Chu et al.*, 2015], as functions of the season of the year [*Tanskanen*, 2009; *Tanskanen et al.*, 2011; *Guo et al.*, 2014], and as functions of the phases of the geomagnetic storms [*Lee and Min*, 2002; *Tanskanen et al.*, 2005].

Substorm-recurrence studies have focused mainly on the periodicity of global sawtooth oscillations, but the criteria discerning global oscillations from ordinary periodic substorms were often not rigorously enforced in the event selections. Hence, some of those global-sawtooth-oscillation studies pertain to periodic substorms in general. The recurrence studies focused on determining the periodicity [*Prichard et al.*, 1996; *Cai and Clauer*, 2009; *Huang et al.*, 2003a, 2003b], on examining the solar wind role in the periodicity [e.g., *Belian et al.*, 1994; *Huang et al.*, 2003a, 2004, 2005; *Lavraud and Borovsky*, 2008; *Partamies et al.*, 2009], and on determining what physically causes the ~3 h periodicity of the magnetosphere [*Belian et al.*, 1994; *Freeman and Morley*, 2004; *Brambles*, 2011, 2013; *Ouellette et al.*, 2013; *Welling et al.*, 2015].

In the present study 28,464 substorms identified with jumps in the SuperMAG *AL* (SML) index in the years 1979–2015 and 16,025 substorms identified with electron injections into geosynchronous orbit in the years 1989–2007 are used to statistically study substorm occurrence rates and substorm recurrence times and their connections to the structure of the solar wind. The study will not be concerned with the "triggering" of substorms by northward turnings of the solar wind magnetic field at rotational discontinuities [e.g., *Rostoker*, 1983; *McPherron et al.*, 1986; *Lyons et al.*, 1997; *Hsu and McPherron*, 2002, 2009; *Freeman and Morley*, 2009], but rather with the occurrences of intervals of enhanced solar wind driving of the magnetosphere.

This report is organized as follows. In section 2 the methodology for determining the occurrence times of substorm onsets is elaborated upon. In section 3 the distributions of substorm recurrence times are analyzed and the relation of substorm recurrence to the structure of the solar wind is examined. In section 4 substorm occurrence rates and substorm recurrence-time distributions are examined for the different phases of the solar cycle and for the different seasons of the year and the Russell-McPherron effect on substorm occurrence rates is examined. In section 5 substorm occurrence rates and substorm recurrence-time distributions are examined for the four different types of solar wind plasma passing the Earth. In section 6 the recurrence time of periodic substorms is examined as functions of substorm amplitude, geomagnetic activity, and solar and solar wind conditions. The findings of this study are summarized in section 7, which also contains discussions about the working picture of substorm occurrence controlled by the solar wind, about the period of periodic substorms, and about global sawtooth oscillations.

2. Event Selection

The strength of auroral-electrojet activity is traditionally characterized by the auroral-electrojet indices *AU* and *AL*. Substorm onset is characterized by an abrupt temporal decrease ("negative bay") in the *AL* index; the decrease is a consequence of an increase of the westward electrojet due to the contribution from horizontal part of the substorm current wedge. The *AL* index is derived from a limited number of

magnetometer stations that have uneven local-time distribution and can detect events only from a specific range of magnetic latitudes. The limited spatial coverage might result in incorrect estimation of substorm onset times and underestimation of substorm occurrence rates when used in statistical studies. An alternative to the *AL* index is the SuperMAG *AL* (SML) index. The difference between SML and *AL* index is in the number of stations used and in methods for establishing the baseline. For this study we use the SML index database from 1979 to 2015 available at http://supermag.jhuapl.edu/indices/. Details of the data and data processing techniques used in the derivation of the SML index are given by *Gjerloev* [2012] and by *Newell and Gjerloev* [2011].

No generally accepted method exists to identify substorm events from auroral electrojet indices, and different sets of criteria were used in different studies [e.g., *Tanskanen et al.*, 2002; *Newell and Gjerloev*, 2011; *Semenov et al.*, 2015; *Forsyth et al.*, 2015]. A prior study by the authors [*Yakymenko and Borovsky*, 2016] highlighted the importance of eliminating the intensification of ongoing substorms from the event selections (see also *Forsyth et al.* [2015]): that report identified event collections that are primarily intensifications (and that do not show a recurrence periodicity) and event collections that are primarily substorm onsets (and that do show a recurrence periodicity). The scheme chosen here is to select robust events in the SML index, with onset times determined by strong negative jumps in the SML index. The criterion used to find onset times is similar to the 100 nT in 10 min criterion used by *Prichard et al.* [1996] to select substorm onset times in the 1 min resolution *AL* index or the 80 nT-in-15 min criterion used by *Tanskanen* [2009] for the *IL* index. The present scheme locates regions where the SML index decreases by at least 150 nT in 15 min, then locates potential onset times within those time intervals where the 2 min change of SML decreases by more than 10 nT (which is a slope of more than −150 nT in 15 min). Then, for each potential onset time, the time integral of the magnitude of the SML index for the 45 min after the onset time is compared with the time integral of the magnitude of the SML index for the 45 min prior to the onset time: if the "after" integral is less than 1.5 times the "before" integral, that onset time is rejected as not representing the onset of a substantial change in geomagnetic activity. (This integral test is designed to eliminate reactivations from the onset list, and the integral test should also eliminate pseudobreakups that are not followed by actual substorms.) The first surviving onset time in each interval where SML decreases by 150 nT or more in 15 min is taken to be the onset of the substorm. Finally, if a 150 nT-in-15 min interval occurs within 15 min of a prior 150 nT-in-15 min interval, the second interval is voided and the onset time in that second interval is not used. To some degree, this eliminates multiple onsets being counted as separate substorms. In this robust-event scheme, the minimum time between substorm onsets in the 1979–2015 SML data set is 27 min. The total number of 28,464 events was selected by the algorithm covering interval from 1979 to 2016. This list of SML-jump events has been submitted as supporting information for this journal article.

Note that no attempt is made to further categorize this list of substorm onsets into subtypes such as global sawtooth oscillations, storm time substorms, or pseudobreakups. This will also be the case below for the list of substorms generated from energetic-electron injections.

The injection of energetic electrons into geosynchronous orbit is temporally associated with the onset of a substorm [e.g., *Kamide and McIlwain*, 1974; *Yeoman et al.*, 1994; *Weygand et al.*, 2008] and is simultaneous with the dipolarization of the nightside magnetosphere at geosynchronous orbit [*Lezniak et al.*, 1968; *DeForest and McIlwain*, 1971; *Sauvaud and Winckler*, 1980; *Birn et al.*, 1998]. An automated method to identify substorm electron injections into geosynchronous orbit was developed based on the observation that the specific entropy $S = T/n^{2/3}$ [cf. *Borovsky and Cayton*, 2011] of the hot-electron population at geosynchronous orbit decreases significantly when a fresh injection of electrons occurs. This entropy decrease is seen as a simultaneous increase of the hot-electron number density and decrease of the hot-electron temperature (hardness of the energy spectrum). When there are no new injections, the population of substorm-injected electrons at geosynchronous orbit ages and the specific entropy of the population steadily increases with time. During this aging, the number density of the electrons decreases with time and the mean energy of the electrons increases with time; this is consistent with less-energetic electrons being lost from geosynchronous orbit at a higher rate leaving a population of more-energetic electrons.

Multispacecraft measurements of energetic electrons from the SOPA (Synchronous Orbit Particle Analyzer) instruments [*Cayton and Belian*, 2007] in geosynchronous orbit are used to determine the specific entropy of the substorm-injected electron population. Specifically, density-temperature fits to the SOPA electron

counting rates for the substorm-injected population are used [*Cayton et al.*, 1989; *Cayton and Belian*, 2007; *Denton et al.*, 2010]. The spin-averaged counting rates for each electron energy channel are modeled as linear combinations of two relativistic Maxwellian components plus a nonelectron "background" contribution; minimizing the squared deviations between the observed and model counting rates summed over 10 electron channels yields the best fit two Maxwellian spectra (see *Cayton and Belian* [2007] for full details). The relativistic bi-Maxwellian fitting describes two populations of electrons: a "soft" population of electrons with a temperature of ~30 keV and a "hard" population of electrons with a temperature of ~150 keV [*Cayton et al.*, 1989; *Denton et al.*, 2010]. The soft population (which is used here) is the suprathermal tail of the electron plasma sheet whose appearance at geosynchronous orbit is associated with substorm injections [*Lezniak et al.*, 1968; *Cayton et al.*, 1989; *Birn et al.*, 1998, 2000]. The hard component is the outer electron radiation belt [*Cayton et al.*, 1989; *Belian et al.*, 1996; *Denton et al.*, 2010]. Density-temperature fits to the electron count rates are made every 10 s for every spacecraft carrying a SOPA detector; from these 10 s resolution fits median values of the temperature and median values of the density are calculated every 30 min on each spacecraft and these 30 min resolution median densities n and median temperatures T are utilized to calculate a specific entropy $S = T/n^{2/3}$ of the substorm-injected electrons with a 30 min resolution for each operating spacecraft. To determine the occurrence of an electron injection at geosynchronous orbit, the minimum value of the quantity $\log_e(S)$ is calculated every 30 min for all of the spacecraft operating at that time; when this multispacecraft-minimum value of $\log_e(S)$ decreases by 1.0 or more in 30 min or in 60 min, an injection is declared. The $\log_e(S)$ decreasing by a factor of 1.0 is equivalent to $\log_{10}(S)$ decreasing by a factor of 0.434 or S decreasing by a multiplicative factor of $e^{-1} = 0.368$. Sometimes the specific entropy continues to decrease for two or more subsequent half-hour intervals. (This could be owed to where in time a sudden decrease in S was captured in the half-hour-resolution medians, or it could be owed to multiple injections during a substorm expansive phase.) If two subsequent half-hour intervals meet the criteria for declaration of an injection, the occurrence of the injection is taken to occur in the first of the two intervals. Hence, in this electron-injection identification scheme, the time between substorm injections is 60 min at the minimum.

Note that the time at which a substorm is detected by using the entropy method depends on the local-time positions of the geosynchronous spacecraft at the time of the actual substorm onset. If no satellite is present in the vicinity of local midnight, then the freshly injected electrons must drift toward dawn and then into the dayside until a satellite is encountered. Hence, the substorm-onset times determined from the SOPA injections are systematically delayed by about 0–0.5 h from the substorm onsets determined by the SML index.

The total number of 16,025 electron-injection events was selected by the algorithm covering interval from 1989 to 2007. This list of electron-injection events has been submitted as supporting information for this journal article.

In general, the two methods identify the same substorms (58% of identified SML-jump onsets have an injection onset proximate in time, and 57% of identified injection onsets have an SML-jump onset proximate in time), but certainly not always. Like thunderstorms that each have different mixes of rain, hail, lightning, wind, and tornadoes, the various amplitude measures of substorms are not completely correlated [*Lopez and von Rosenvinge*, 1993; *Borovsky and Nemzek*, 1994]; hence, the various detection methods for substorms will select different events.

3. Substorm Recurrence-Time Distributions

The substorm recurrence time (waiting time) Δt is the time interval from the onset of one substorm to the onset of the next substorm. In Figure 1 the occurrence distribution of recurrence times is plotted for substorm onsets determined by jumps in the SML index in the years 1979–2015 (blue curve) and for substorm onsets determined by electron injections into geosynchronous orbit in the years 1989–2007 (red curve). The recurrence-time distributions for electron injections and for SML jumps are similar to each other. The recurrence-time distributions in Figure 1 are similar to substorm recurrence-time distributions found in previous studies [e.g., *Borovsky et al.*, 1993, Figures 3 and 4; *Prichard et al.*, 1996, Figure 1], which were composed of a quasi-Gaussian population centered on about 3 h and an exponential distribution at larger Δt values. Owing to the larger number of substorms used in the present study, the distributions in Figure 1 extend to much larger values of Δt than prior distributions did.

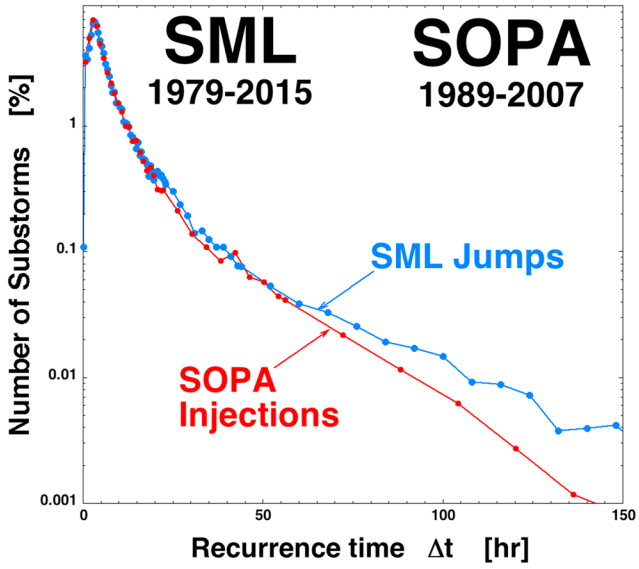

Figure 1. The recurrence-time distributions of substorm onsets for 28,464 substorms identified with jumps in the SML index in 1979–2015 (blue) and for 16,025 substorms identified with electron injections into geosynchronous orbit in 1989–2007 (red).

In Figure 2 the SML recurrence-time distribution from Figure 1 is mathematically analyzed. The distribution from the SML data is plotted in black. For recurrence times $30\,\mathrm{h} < \Delta t < 165\,\mathrm{h}$ the black curve is fit by an exponential function and

$$\mathrm{fit1} = 0.328\ \exp(-\Delta t/31.4\,\mathrm{h}) \quad (1)$$

results. This exponential fit is plotted as the orange curve in Figure 2. Subtracting fit1 off of the black curve for all values of Δt, the blue curve results. For recurrence times $8\,\mathrm{h} < \Delta t < 24\,\mathrm{h}$ the blue curve is fit by the exponential function

$$\mathrm{fit2} = 4.84\ \exp(-\Delta t/6.76\,\mathrm{h}), \quad (2)$$

which is plotted as the red curve in Figure 2. The green curve in Figure 2 is the blue curve with fit2 subtracted off for all values of Δt. Hence, the green curve in Figure 2 is the recurrence-time distribution (black) with the two exponential fits subtracted off. A similar analysis was performed in *Borovsky et al.* [1993], wherein a single exponential function was subtracted off of the recurrence-time distribution and the quasi-Gaussian residual (i.e., the green curve) was interpreted to be recurrence times for a population of quasiperiodically occurring substorms. The information-theoretic analysis of *Prichard et al.* [1996] confirmed that interpretation. In *Borovsky et al.* [1993] it was noted that an exponential distribution of recurrence times is consistent with random occurrence of substorms following a Poisson process wherein the probability of substorm occurrence is independent of the past record of occurrence [*International Telegraph and Telephone Corporation*, 1979].

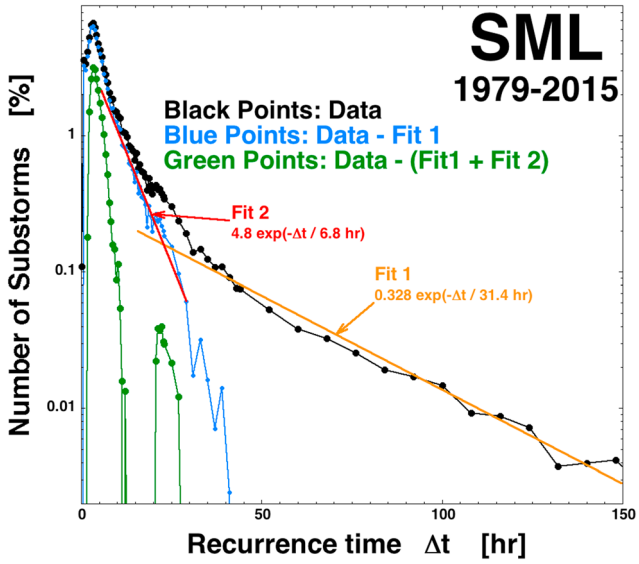

Figure 2. The recurrence-time distribution for 28,464 substorms identified with jumps in the SML index in 1979–2015 is mathematically analyzed into three populations.

The following interpretation is made of the residual distribution (green curve) and the two exponential fits of Figure 2. (1) The residual waiting-time distribution (green curve) represents the recurrence of substorms in a periodic fashion with a substorm-recurrence period of 2–4 h. (2) The exponential distribution (fit2) of recurrence times of expression (2) represents the occurrence of substorms associated with random occurrences of solar wind intervals capable of driving the magnetosphere sufficiently to create a substorm; we will look for evidence that the time scale of 6.8 h of this fit is associated with the mesoscale magnetic structure of the solar wind. (3) The exponential distribution (fit1) of recurrence times of expression (1) represents the durations of intervals

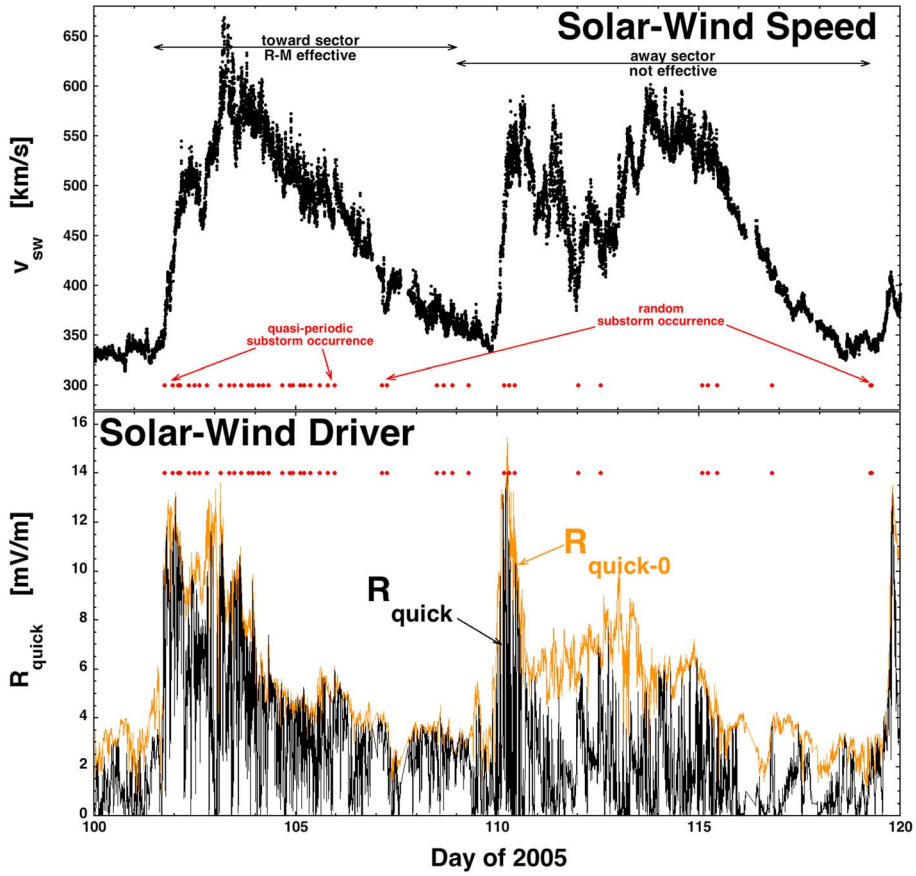

Figure 3. For 20 days in the spring of 2005 the occurrence of substorms (red dots) is examined in comparison with (top) the speed of the solar wind and (bottom) the strength of solar wind driving of the magnetosphere.

of the solar wind wherein it is probable that the driving of the magnetosphere is too weak to produce a substorm; we will look for evidence that the 34.5 h time scale of this fit is associated with the large-scale structure of the solar wind plasma.

Figure 3 demonstrates some aspects of the periodic occurrence of substorms versus the random occurrence of substorms. In Figure 3 (top) the solar wind velocity is plotted for 20 days in the spring of the year 2005; two high-speed streams are contained in the 20 day interval. In Figure 3 (bottom) the solar wind driver function R_{quick} is plotted (black). R_{quick} is derived [*Borovsky and Birn*, 2014] to represent the reconnection rate (in units of mV/m) at the nose of the magnetosphere based on the Cassak-Shay equation [*Cassak and Shay*, 2007] for the reconnection rate between two collisionless magnetized plasmas (the magnetosphere and the magnetosheath). R_{quick} is (in MKS units)

$$R_{quick} = 2.04\,\mu_o^{1/2} m_p^{1/2} n_{sw}^{1/2} v_{sw}^{2} \sin^2(\theta_{clock}/2)\, M_A^{-1.35}\left[1 + 680 M_A^{-3.30}\right]^{-1/4}, \quad (3)$$

where n_{sw} is the solar wind proton number density, v_{sw} is the solar wind velocity, θ_{clock} is the IMF clock angle with respect to the Earth's magnetic dipole, and $M_A = v_{sw}/v_A$ is the solar wind Alfven Mach number, with $v_A = B_{sw}/(4\pi m_p n_{sw})^{1/2}$ being the Alfven speed in the upstream solar wind. The formula for R_{quick} can be separated into two parts:

$$R_{quick} = R_{qo} \sin^2(\theta_{clock}/2) \quad (4a)$$

$$R_{qo} = 2.04\,\mu_o^{1/2} m_p^{1/2} n_{sw}^{1/2} v_{sw}^{2} M_A^{-1.35}\left[1 + 680 M_A^{-3.30}\right]^{-1/4}, \quad (4b)$$

where m_p is the mass of a proton, R_{qo} represents the portion of R_{quick} that is associated with the structure of the solar wind plasma (n_{sw}, B_{sw}, and v_{sw}), and $\sin^2(\theta_{clock}/2)$ is the portion of R_{quick} that is associated with the

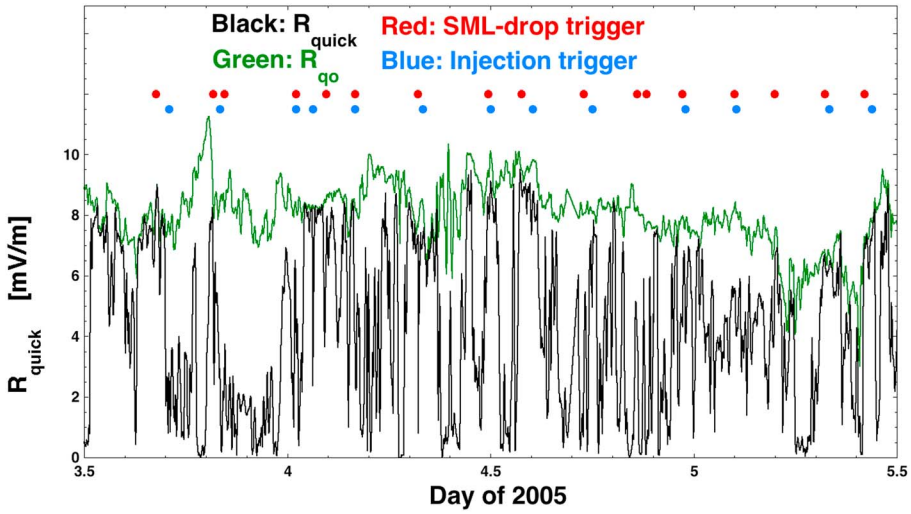

Figure 4. For 2 days in 2005 the occurrence of quasiperiodic substorms (red and blue dots) is compared with the driving of the magnetosphere by the solar wind (black curve).

magnetic field-vector structure of the solar wind. In Figure 3 (bottom) R_{qo} is plotted in blue for the 20 days. In both panels of Figure 3 the occurrence times of substorm onsets as determined by jumps in the SML index are indicated by red dots. As indicated in Figure 3 (top)there is an interval wherein substorms occur in a quasiperiodic fashion (days 102–105) and an interval wherein substorms occur in a random fashion (days 107–118). In Figure 3 (top) an interval wherein the IMF sector is in a toward orientation and an interval wherein it is in and away sector are indicated. According to the Russell-McPherron effect [*Russell and McPherron*, 1973], the solar wind tends to be more geoeffective in the spring season when the IMF is in a toward sector and tends to be not geoeffective in the spring season when the IMF is in an away sector. This is reflected in Figure 3 (bottom) wherein R_{quick} (black) is larger in the first high-speed stream (toward sector) than it is in the second high-speed stream (away sector). In Figure 3 the periodic substorms are occurring when the solar wind driver (i.e., R_{quick}) is high for a sustained interval and the substorms are randomly occurring when the solar wind driving is weaker.

Note that the same conclusions as those from Figure 3 result if another solar wind driver such as the Newell function $v_{sw}{}^{4/3}B_{perp}{}^{2/3}\sin^{8/3}(\theta_{clock}/2)$ [*Newell et al.*, 2007] is used, with that function separated into a plasma term $v_{sw}{}^{4/3}B_{perp}{}^{2/3}$ and a magnetic-clock-angle term $\sin^{8/3}(\theta_{clock}/2)$.

Figure 4 focuses on an interval of quasiperiodic substorm occurrence in the year 2005. Two days are displayed. The solar wind driving function R_{quick} is plotted in black, and the plasma component R_{qo} of R_{quick} is plotted in green. The occurrence times of substorms as determined by jumps in the SML index are indicated in red, and the occurrence times of substorms as determined by electron injections are indicated in blue. Note that injection times are delayed by 0–30 min owing to the local-time positions of spacecraft in geosynchronous orbit at the time of the actual substratum onset. In Figure 4 R_{quick} is highly time varying compared with R_{qo}: this is because of rapid variations in $\sin^2(\theta_{clock}/2)$ (cf. expressions (4a) and (4b)) that are owed to rapid variations in θ_{clock}, the direction of the solar wind magnetic field. The rapid time variations in R_{quick} are caused by the mesoscale spatial structure of the solar wind magnetic field being advected past the Earth producing rapid changes in θ_{clock}. Note that the variations in R_{quick} occur more rapidly than the recurrence times between the substorm onsets.

In Figure 5 the superposed-epoch average of the solar wind driver function R_{quick} is plotted as a function of time where the zero epoch (trigger) is the occurrence time of substorm onset as determined by the jump in the SML index. The substorm onsets are separated into two groups: random substorms (where the time since the prior substorm is 6 h or more) and periodic substorms (where the time since the prior substorm is between 2 and 4 h). In Figure 5 (top) the superposed average of R_{quick} is plotted in blue for the group of periodic substorms and the superposed average of R_{quick} is plotted in red for the group of random substorms.

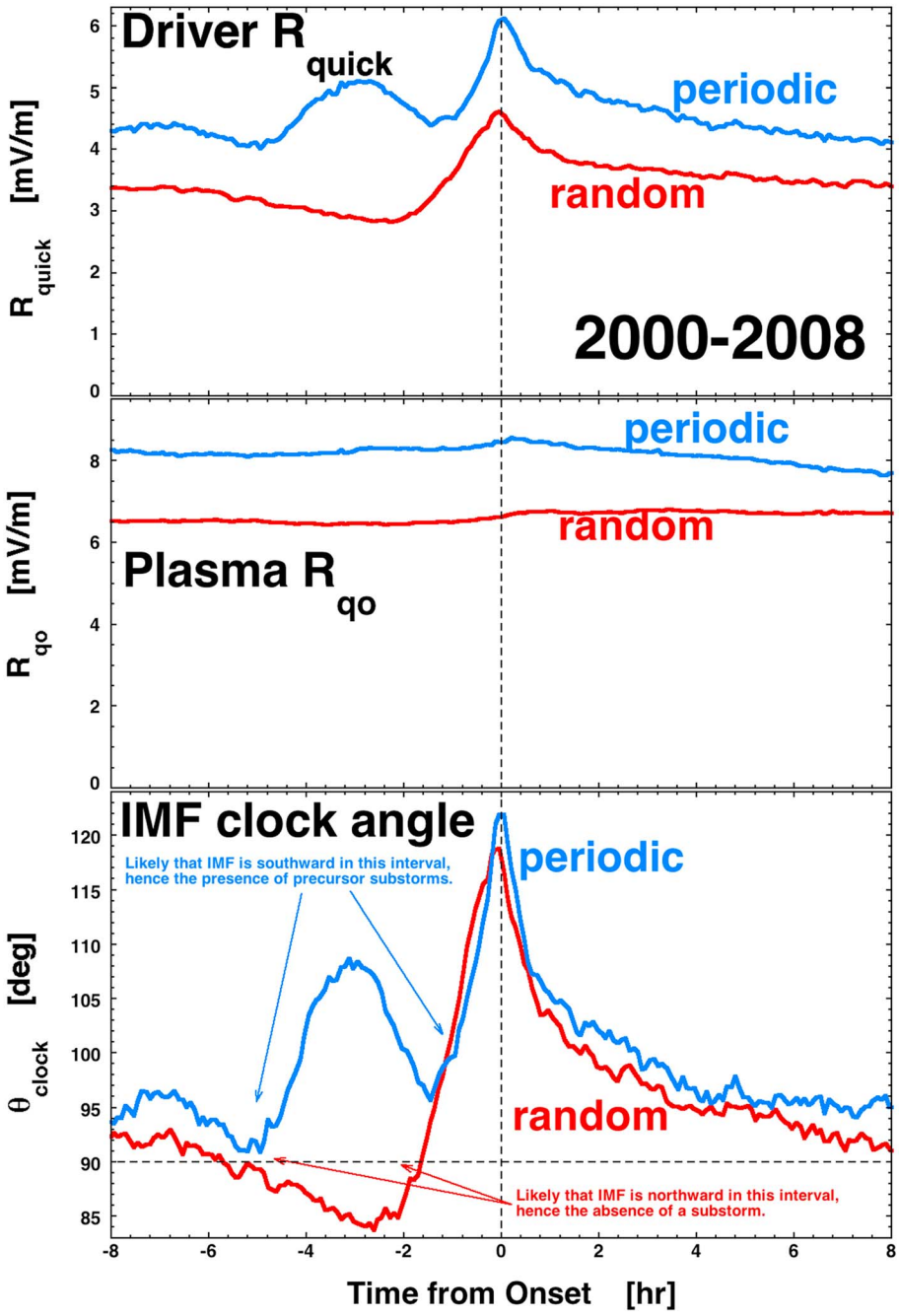

Figure 5. The driving of the magnetosphere by the solar wind is examined using superposed-epoch averaging triggered on the times of substorm onsets as determined by the jumps in the SML index in 2000–2008. The substorms are separated into two populations: periodic (blue curves) and random (red curves). (top) The superposed average of the solar wind driver R_{quick} is plotted, (middle) the plasma portion R_{qo} of R_{quick} is plotted, and (bottom) the clock angle of the IMF is plotted.

Both curves in Figure 5 (top) indicate that substorm onset is associated with an interval of enhanced solar wind driving prior to the onset [e.g., *Fairfield and Cahill*, 1966; *Caan et al.*, 1977, 1978; *Morley and Freeman*, 2007; *Wild et al.*, 2009] (and see in particular the superposed-epoch analysis of *Newell and Liou* [2011]). In Figure 5 (middle) the plasma portion R_{qo} of R_{quick} is plotted for the two sets of triggers: note that the substorm onset occurrence is not associated with a variation in the solar wind plasma properties. In Figure 5 (bottom) the superposed average of the IMF clock angle θ_{clock} is plotted for the two sets of

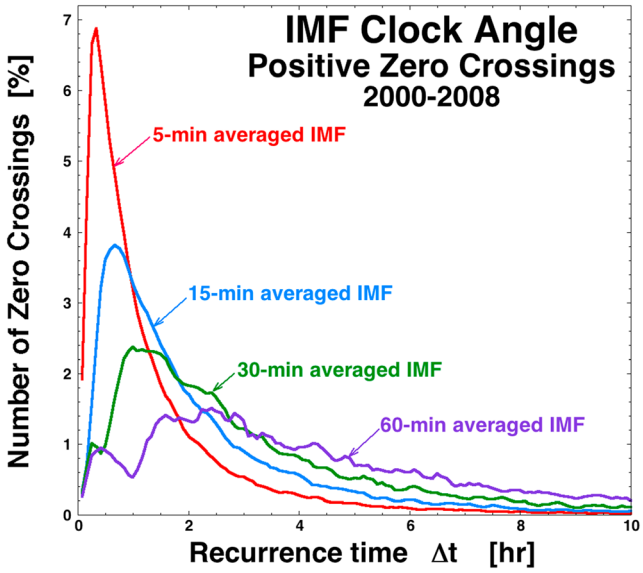

Figure 6. The waiting-time distributions for crossings of the IMF clock angle through 90° going southward are binned. Each colored curve uses a different time averaging of the 5 min resolution OMNI2 data set.

triggers: both the periodically occurring (blue) and the randomly occurring (red) substorms are temporally associated with an increase in the IMF clock angle θ_{clock} at the time of the substorm onset. Note that for the red curve (randomly occurring substorms) in Figure 5 (bottom) that θ_{clock} is on average less than 90° (northward IMF) in the interval prior to the occurrence of the substorm, whereas for the blue curve (periodically occurring substorms) that θ_{clock} is on average greater than 90° (southward) in the interval before the substorm occurs. This agrees with the idea that random substorms tend to occur during intervals of weaker driving and that periodic substorms occur during intervals of stronger driving (cf. Figure 3). The two curves plotting R_{qo} in Figure 5 (middle) also indicate this random substorms during weaker driving and periodic substorms during stronger driving. Note in the blue curves for periodic substorms in Figure 5 (top and bottom) that there is an indication of enhanced driving 2–4 h prior to the occurrence of the substorm at the zero epoch: this indicates that the prior substorms (which occurred by definition 2–4 h earlier) are also associated with an interval of enhanced driving (caused by an interval of more-southward IMF clock angle). This plot raises the question: is the ~3 h periodicity of substorm occurrence caused by an ~3 h periodicity in the solar wind producing a 3 h periodicity in the driving of the magnetosphere or is it caused by an inherent property of the magnetosphere-ionosphere system?

To investigate whether there is an ~3 h periodicity in the driving of the Earth by the solar wind, Figure 6 explores some time scales in the solar wind time series at Earth. Using 5 min averages of the advected solar wind magnetic field from the OMNI2 database [*King and Papitashvili*, 2005], the clock angle θ_{clock} of the IMF is calculated at Earth as a function of time for the 9 years (2000–2008). The zero crossings of the time series [e.g., *Ylvisaker*, 1965; *Sreenivasan et al.*, 1983] are determined wherein the clock angle θ_{clock} crosses from less than 90° (northward) to greater than 90° (southward) and the time intervals Δt between the zero crossings are calculated. The waiting-time distribution for the zero crossings for the 5 min averaged θ_{clock} is plotted in red in Figure 6. The 5 min resolution values of θ_{clock} are time averaged to 15 min, the zero crossings in the 15 min time series are located, and the waiting-time distribution of the 15 min averaged θ_{clock} values is plotted as the blue curve in Figure 6. The process is repeated for 30 min averages of θ_{clock} and for 60 min averages of θ_{clock}, and the waiting-time distributions for the zero crossings are plotted in green and purple, respectively, in Figure 6. The red curve in Figure 6 represents the occurrence distribution of times between the onsets of intervals of driving that are 5 min or more in length. Similarly, the blue curve in Figure 6 represents the occurrence distribution of waiting times between the onsets of driving intervals that are 15 min in length; the green curve represents the occurrence distribution of waiting times between the onsets of driving intervals that are 30 min in length, and the purple curve represents the occurrence distribution of waiting times between the onsets of solar wind driving intervals that are 60 min in length. In Figure 6 there is no indication of an ~3 h periodicity in the occurrence of driving intervals in the solar wind. If R_{qo} of the solar wind is strong, southward IMF intervals occur more frequently than 3 h and intervals of enhanced driving will occur more frequently than the ~3 h periodicity of substorm occurrence (cf. Figure 4). A working model of the occurrence of periodic substorms is that the periodicity of substorm occurrence is 2–4 h because of some inherent property of the magnetosphere-ionosphere system and that a substorm will occur after this "magnetospheric" interval

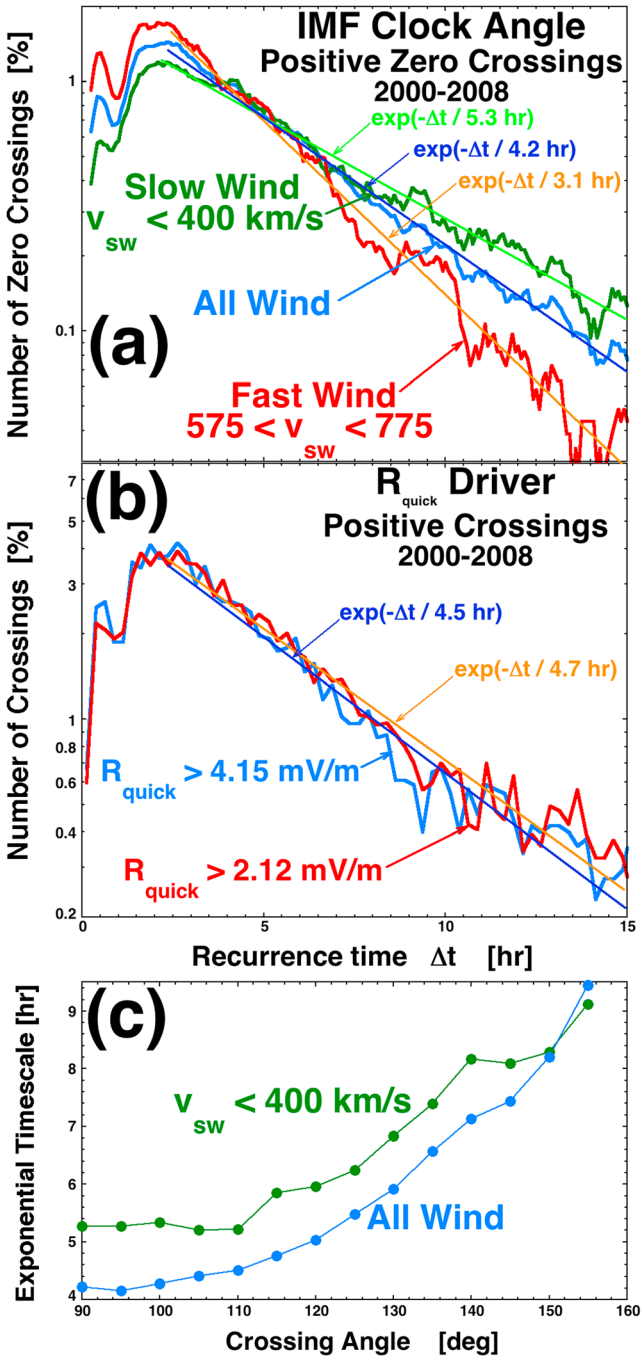

Figure 7. (a) For 60 min averages of the 5 min resolution OMNI2 data set, the waiting times for the 90° crossings of the IMF clock angle are binned: the blue curve is for all solar wind, the green curve is for slow solar wind ($v_{sw} < 400$ km/s), and the red curve is for fast solar wind (v_{sw} in the range of 575–775 km/s). Exponential fits to the three curves are shown. (b) For 60 min averages of the 5 min resolution OMNI2 data set, the waiting times for positive crossings of two values of the driver function R_{quick} are binned: the blue curve is for crossings of $R_{quick} = 4.15$ mV/m, and the red curve is for crossings of $R_{quick} = 2.12$ mV/M. Exponential fits to the two curves are shown. (c) The exponential fit parameters to the clock-angle waiting-time distributions are shown for the all solar wind (blue) and for the slow solar wind (green) as the crossing angle is varied from 90° to 155°.

when the next available solar wind-driving interval occurs. Hence, the variability of the recurrence period is caused by the added waiting time for a solar wind-driving interval.

Solar wind time scales associated with the random occurrence of substorms are examined in Figure 7. The clock-angle zero-crossing waiting-time distributions plotted in Figure 6 are actually well fit by exponential distributions. In Figure 7a the 60 min averaged distribution from Figure 6 is replotted (blue curve) logarithmically and fit with an exponential function $\exp(-\Delta t/4.2\,\text{h})$. Hence, the 60 min average of the magnetic field vector of the solar wind has random southward crossings (through $\theta_{clock} = 90°$) randomly with a characteristic time scale of 4.2 h between subsequent crossings. The solar wind zero-crossing waiting times are separately collected for intervals of typical slow wind ($v_{sw} < 400$ km/s) and for intervals of typical fast wind ($v_{sw} = 575$–775 km/s), and those distributions are plotted in green and red, respectively, in Figure 7a. The time scales of magnetic structure as seen by the Earth are shorter in the red curve of the fast wind (coronal-hole plasma) than they are in the green curve of the slow wind; the mesoscale magnetic structures of the slow wind are larger than the structures of the fast wind [*Borovsky*, 2008], and the slow wind advects the structures past the Earth at a slower rate. The slow-wind waiting-time distribution is fit by $\exp(-\Delta t/5.3\,\text{h})$, and the fast-wind waiting-time distribution is fit by $\exp(-\Delta t/3.1\,\text{h})$. Similarly, in Figure 7b the waiting-time distributions for crossings of the magnetospheric driver function R_{quick} are plotted and fitted. The red curve is the distribution of waiting times for the hourly average of R_{quick} to exceed 2.12 mV/m (which is the median value of R_{quick}), and the blue curve is the distribution of waiting times for the hourly average of

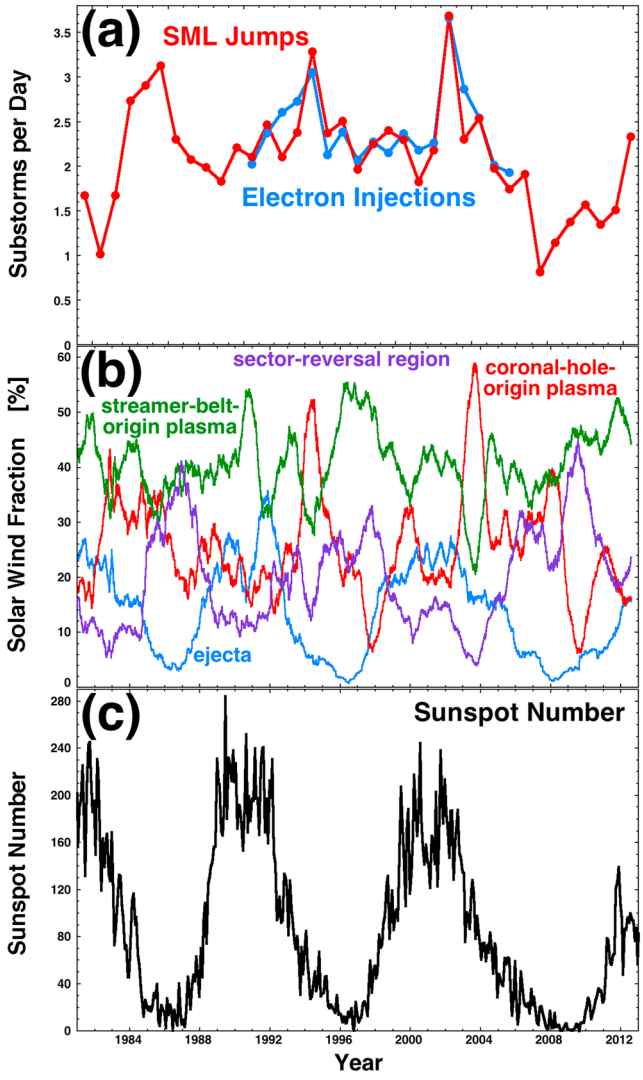

Figure 8. (a) The substorm occurrence rate (substorms per day) is plotted as functions of time for three solar cycles; the red curve is for substorms determined by jumps in the SML index, and the blue curve is for substorms determined by electron injections. (b) In a 1 year running average of the fraction of time four different types of solar wind are seen at Earth, as determined from the parameters of the OMNI2 solar wind data set. (c) The monthly sunspot number is plotted.

R_{quick} to exceed 4.15 mV/m (which is the 75% quartile of R_{quick}). The exponential fit distributions for R_{quick} waiting times in Figure 7b yield similar waiting times as the southward crossings through $\theta_{clock} = 90°$) in Figure 7a. The fits in Figure 7a are for crossings southward across $\theta_{clock} = 90°$. If the zero line for the zero crossings is taken at larger values of θ_{clock} (i.e., more southward values), the waiting times are longer and the distribution has a different characteristic time scale. In Figure 7c the exponential fitting of the top plot is repeated for zero-crossing waiting-time distributions where the crossing angle is varied from $\theta_{clock} = 90°$ to $\theta_{clock} = 155°$. As the requirement for an interval of IMF is more south (greater θ_{clock}), the characteristic time of the exponential fit to the waiting-time distribution increases. The characteristic time scale of the exponential waiting-time distribution of substorms onsets (6.8 h in Figure 2) is in the vicinity of the characteristic time scales of the exponential waiting-time distributions of solar wind-driving intervals in Figure 7c, particularly for slow solar wind where the randomly occurring substorms are prominent. Hence, the statistics support the picture articulated by *Morley and Freeman* [2007], wherein the randomly occurring substorms are associated with randomly occurring intervals of good solar wind driving (associated with randomly occurring intervals of the direction of the solar wind magnetic field at Earth).

4. Phase of the Solar Cycle and Season of the Year

In Figure 8a the substorm occurrence rates (in unit of substorms per day) as determined from jumps in the SML index (red curve) and as determined from electron injections (blue curve) are plotted as a function of time for the years 1979 to 2015. Each point is the average value for a calendar year. In Figure 8c the monthly sunspot number is plotted. The substorm occurrence rate varies from year to year, and the two measures of substorm occurrence track each other fairly well. As is known [cf. *Nevanlinna and Pulkkinen*, 1998; *Tanskanen*, 2009; *Tanskanen et al.*, 2011], the substorm occurrence rate is greatest in the declining phase of the solar cycle. During the declining phases of the solar cycle equatorward extensions of coronal holes on the Sun can have geometries that result in long-lived high-speed coronal-hole-origin plasma at Earth [cf. *McAllister et al.*, 1996]; early in the declining phase (near solar maximum) high-speed ejecta can also enhance the

Table 1. Substorm-Occurrence Rates for the Various Phases of the Solar Cycle

	SML Jumps per Year	SML Jumps per Day	Injections per Year	Injections per Day
Solar maximum	723	1.99	842	2.31
Declining phase	1014	2.78	1028	2.81
Solar minimum	688	1.88	779	2.13
Ascending phase	641	1.85	809	2.22
All times	769	2.11	886	2.43

early phases of high-speed-stream-driven storms. Note that the substorm occurrence rate was very low in the year 2009, which was an interval of exceptionally weak solar wind [cf. *Smith et al.*, 2013; *Zerbo and Richardson*, 2015]. Note that the SML index for 1979 and 1980 had a sparcity of stations, which may account for the low substorm occurrence rates registered for those years in the red curve. In a 1 year running average of the fraction of time four different types of solar wind plasma are at Earth, as determined by the *Xu and Borovsky* [2015] solar wind categorization scheme applied to the OMNI2 solar wind data set (Figure 8b).

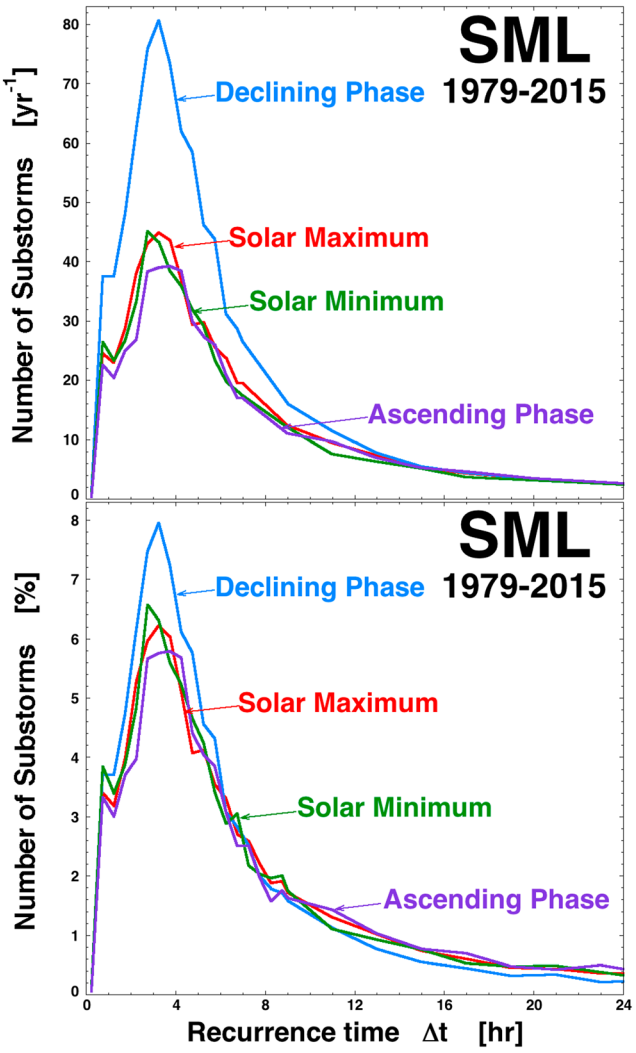

Figure 9. The recurrence-time distributions for substorms as determined by jumps in the SML index in 1979–2015 are plotted for the four phases of the solar cycle. (top) The area under each curve is the number of substorms per year, which differs for the different phases of the solar cycle (cf. Table 1). (bottom) The areas under the curves are all the same.

In Table 1 the substorm-occurrence rates as determined by jumps in SML and by electron injections are collected for the four phases of the solar cycle. (Note that the SML substorms and the injection substorms have different ranges of years, a seen in Figure 8.) Rates are given in units of substorms per year and substorms per day. The bottom line of Table 1 displays the substorm-occurrence rates for all phases of the solar cycle.

In Figure 9 the recurrence-time distributions for substorms as determined by jumps in the SML index are plotted for the four seasons of the solar cycle. In Figure 9 (top) the area under each curve is the number of substorms per year (cf. Table 1), and in Figure 9 (bottom) the areas under the four curves are all equal (the areas each being 100%). The declining phase of the solar cycle exhibits increased rates of substorm occurrence (cf. Table 1): the blue curve in Figure 9 (top) indicates that much of this increase in occurrence during the declining phase is an increase in the occurrence of periodic substorms centered on $\Delta t \sim 3$ h. The blue curve in Figure 9 (top) also exhibits an increase in the rate of randomly occurring substorms with Δt greater than about 7 h. In Figure 9 (bottom) it is seen

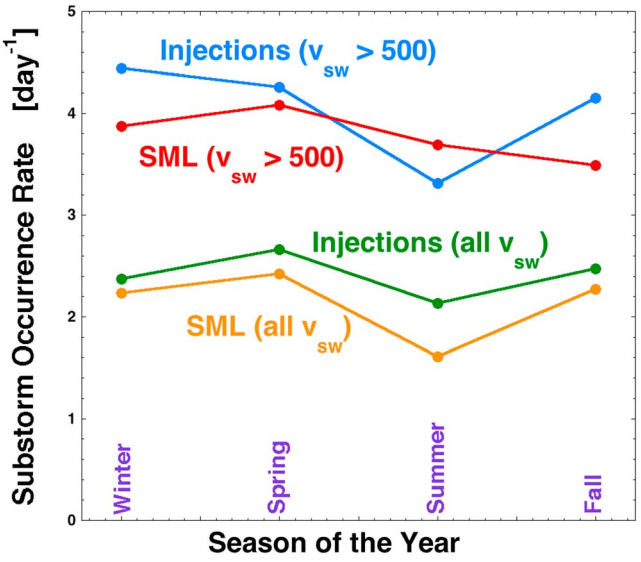

Figure 10. The substorm occurrence rates (substorms per day) are plotted for the four intervals around the equinoxes and solstices of the year. The lower two curves are the occurrence rates at all times, and the upper two curves are the occurrence rates when the velocity of the solar wind exceeds 500 km/s. As labeled, two curves are for substorms as determined with jumps in the SML index in 1979–2015 and two curves are for substorms determined with electron injections in 1989–2007.

that the fraction of substorms that are periodic ($\Delta t = 2$–4 h) is higher for the declining phase and that the fraction of substorms that are random ($\Delta t >$ about 7 h) is smaller. Both panels of Figure 9 indicate that the distributions of substorm recurrence times Δt are similar to each other in the other three phases (solar maximum, solar minimum, and the ascending phase) of the solar cycle.

In Figure 10 the substorm occurrence rate (number of substorms per day) is plotted as a function of the equinoctial season of the year. In the plot winter is the approximately 91 daylong interval centered about the winter solstice (from days 309 to 34), spring is the approximately 91 daylong interval centered about the spring equinox (from days 34 to 126), summer is the approximately 91 daylong interval centered about the summer solstice (from days 126 to 218), and fall is the approximately 91 daylong interval centered about the fall equinox (from days 218 to 309). The substorm occurrence rate derived from jumps in the SML index is plotted in orange, and the occurrence rate as determined by electron injections is plotted in green. (The values of these two curves are collected in Table 2.) The occurrence rates when the solar wind velocity is greater than 500 km/s are plotted in red and blue for SML events and injection events. Examining the orange and green curves in Figure 10, it is seen that the rate of substorm occurrence is slightly less in summer then it is in the other three seasons. This summer deficit has been noted before [e.g., *Borovsky and Nemzek*, 1994; *Tanskanen*, 2009; *Tanskanen et al.*, 2011; *Guo et al.*, 2014]. Note that *Tanskanen* [2009] and *Tanskanen et al.* [2011], using the IMAGE magnetometer chain in Scandinavia to identify substorms, found that the summer occurrence rate was only about half of the winter occurrence rate: the summer depletion found here using SML jumps and using electron injections is not nearly that strong. Examining the red and blue curves of Figure 10, the summer minimum in the substorm occurrence rate is seen for the $v_{sw} > 500$ km/s time intervals in the injection-identified substorms but not in the SML-identified substorms.

In Figure 11 the analysis of Figure 10 is repeated separating the solar wind data into toward magnetic sectors (solid curves) and away magnetic sectors (dashed curves). The toward versus away nature of the solar wind was determined on an hourly basis by taking the dot product of the hourly averaged solar wind magnetic field vector and the hourly average velocity-dependent Parker-spiral-direction vector. The sign of the dot product determines the toward versus away nature of the solar wind interval during the occurrence of each

Table 2. Substorm-Occurrence Rates (in Units of Substorms per Day) Are Collected for the Seasons of the Year and for Toward and Away Magnetic Sectors of the Solar Wind

	Toward Sectors		Away Sectors		All Data	
Equinox	SML Jumps	Injections	SML Jumps	Injections	SML Jumps	Injections
Winter	1.91	1.97	2.36	2.76	2.23	2.37
Spring	2.67	2.92	1.97	2.18	2.42	2.66
Summer	1.61	2.18	1.52	2.07	1.61	2.13
Fall	1.80	1.94	2.40	2.71	2.27	2.47

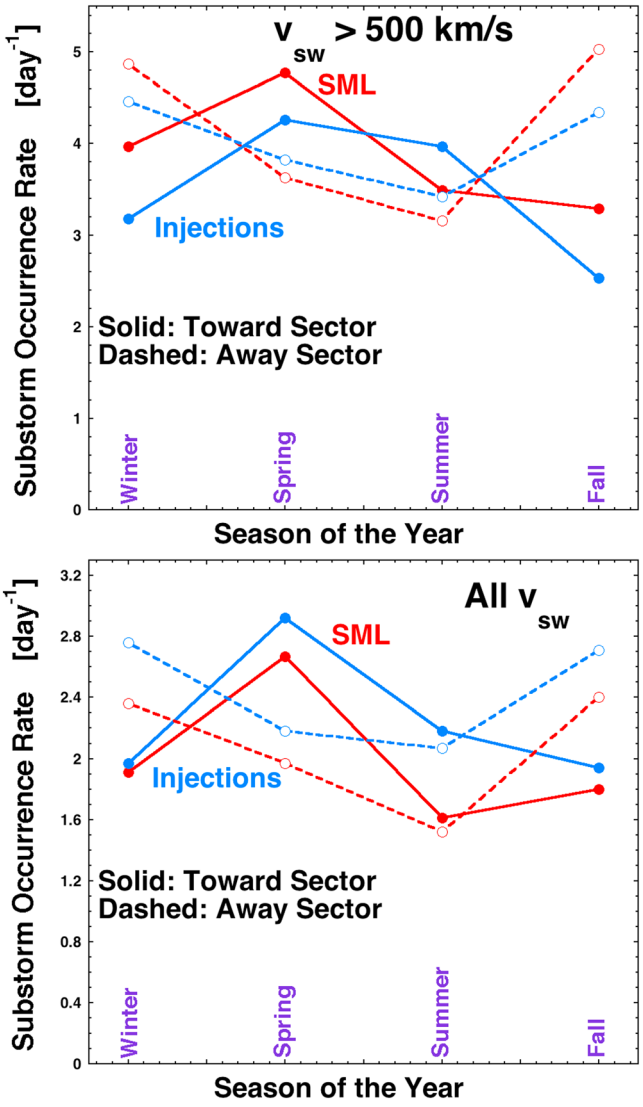

Figure 11. The substorm occurrence rates (substorms per day) are plotted for the four intervals around the equinoxes and solstices of the year, separating the time intervals into toward and away magnetic sectors for the solar wind at Earth. (bottom) The occurrence rates at all times and (top) the occurrence rates when the velocity of the solar wind exceeds 500 km/s are plotted. The red curves are for substorms as determined with jumps in the SML index in 1979–2015, the blue curves are for substorms determined by electron injections in 1989–2007, the solid curves are for toward magnetic sectors, and the dashed curves are for away magnetic sectors.

substorm onset. Note that this method of determining toward versus away sectors is not foolproof owing to (1) large-amplitude directional variations of the solar wind magnetic field about the Parker-spiral direction [cf. *Borovsky*, 2010parker] and to (2) ejecta which is neither toward nor away [*Bame et al.*, 1981; *Borovsky*, 2010]. A superior method for determining toward versus away magnetic orientations is to use the direction of the energetic-electron strahl [e.g., *Kahler and Lin*, 1994; *Crooker et al.*, 2004]; unfortunately, electron strahl measurements at Earth are not readily available prior to 1995. For the total substorm occurrence rates (Figure 11, bottom) and for the occurrence rates during times when $v_{sw} > 500$ km/s (Figure 11, top) a Russell-McPherron effect [*Russell and McPherron*, 1973] is clearly seen wherein geomagnetic activity is enhanced during toward sectors in spring and during away sectors in fall and is suppressed during away sectors in spring and during toward sectors in fall. (The values from Figure 11 (bottom) are collected in Table 2.) The Russell-McPherron effect in the occurrence rate of substorms has been seen before [*Borovsky and Nemzek*, 1994], where it was noted that the effect is not strong; in Figure 11, the Russell-McPherron effect is a tens of percent effect on the rate of substorm occurrence. For the spring and fall seasons the ratios of the Russell-McPherron-enhanced substorm-occurrence rates to the Russell-McPherron-suppressed substorm-occurrence rates are in the range of 1.33 to 1.40.

5. The Type of Solar Wind Plasma

In Table 3 the substorm occurrence rates (number of substorms per day) as determined by SML jumps and by electron injections are displayed for the four types of solar wind plasma. Using the *Xu and Borovsky* [2015] solar wind categorization scheme, the OMNI2 data set [*King and Papitashvili*, 2005] is categorized as to whether the solar wind plasma passing the Earth is of (a) coronal-hole origin, (b) streamer-belt origin, (c) sector-reversal-region origin, or (d) ejecta. (Ejecta also includes magnetic clouds.) Table 3 indicates that there is a great difference in the substorm occurrence rates between the different types of solar wind plasma. The occurrence rate is highest by far in coronal-hole-origin plasma, which is colloquially known as the "fast wind."

Table 3. Substorm-Occurrence Rates (in Units of Substorms per Day) Are Collected for the Four Types of Solar-Wind Plasma at Earth

Type of Solar Wind	Occurrence Rate Using SML Jumps	Occurrence Rate Using Electron Injections
Coronal-hole-origin plasma	3.82	3.72
Streamer-belt-origin plasma	1.72	2.09
Sector-reversal-region plasma	0.91	1.26
Ejecta plasma	1.95	2.32
All types of plasma	2.11	2.43

The substorm occurrence rate is lower in streamer-belt-origin plasma, and the rate is very low (well below average) in sector-reversal-region plasma. The occurrence rate is about average in ejecta plasma. As noted in *Xu and Borovsky* [2015, Figure 21], coronal-hole-origin plasma is prevalent during the declining phase of the solar cycle, which according to Table 1 and Figure 8 exhibits a higher-than-normal substorm occurrence rate. Undoubtedly, the difference in the substorm occurrence rates has to do with the average levels of solar wind driving of the magnetosphere in the four types of solar wind plasma, with coronal-hole-origin plasma leading, on average, to stronger levels of driving.

The distributions of substorm recurrence times in the four types of solar wind plasma are displayed in Figure 12, where the type of solar wind plasma is again determined with the *Xu and Borovsky* [2015] categorization scheme. The areas under the four curves in Figure 12 are all equal. Note in the red curve the dominance of the occurrence of periodically occurring substorms ($\Delta t \sim 2$–4 h) relative to the randomly occurring substorms (Δt greater than about 6 h) in coronal-hole-origin plasma; note the opposite trend in the purple curve for sector-reversal-region plasma where the periodically occurring substorms are sparse. The large Δt tail of the sector-reversal-region plasma (purple curve) is robust and (not shown) dominates the large Δt tails of the other curves beyond 24 h. This indicates that long intervals of time without the occurrence of a substorm are common in sector-reversal-region plasma. For streamer-belt-origin plasma (green curve) and ejecta plasma (blue curve) periodic substorms are common, as are randomly occurring substorms.

6. The Substorm Recurrence Period

The ~3 h periodicity of substorm (and global-sawtooth-oscillation) recurrence is well known [e.g., *Borovsky et al.*, 1993; *Belian et al.*, 1994, 1995; *Prichard et al.*, 1996; *Huang et al.*, 2003a; *Borovsky*, 2004; *Henderson et al.*, 2006b; *Cai and Clauer*, 2009; *Morley and Henderson*, 2010; *Hsu and McPherron*, 2012; *Noah and Burke*, 2013]. The physical processes and controlling parameters that determine the periodicity of substorm recurrence have been a mystery for decades [e.g., *Belian et al.*, 1994; *Huang et al.*, 2003a; *Borovsky*, 2004; *Freeman and Morley*, 2004; *Morley and Henderson*, 2010; *Cai and Clauer*, 2009; *Brambles et al.*, 2013; *Ouellette et al.*, 2013; *Welling et al.*, 2015]. Using the large numbers of substorms obtained from the jumps in the SML index in the years 1979–2015 and from electron injections into geosynchronous orbit in the years 1989–2007, the periodicity of substorm recurrence is investigated in this section as functions of substorm amplitude, geomagnetic activity, and solar and solar wind conditions.

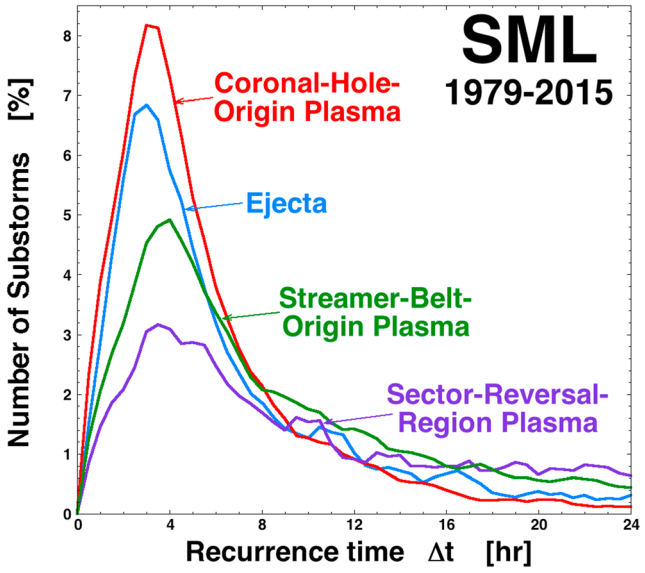

Figure 12. For 36 years, the recurrence-time distribution for substorms determined from jumps in the SML index is plotted separately for intervals of time when the solar wind plasma at Earth is of coronal-hole origin (red), streamer-belt origin (blue), sector-reversal-region origin (purple), and ejecta (blue).

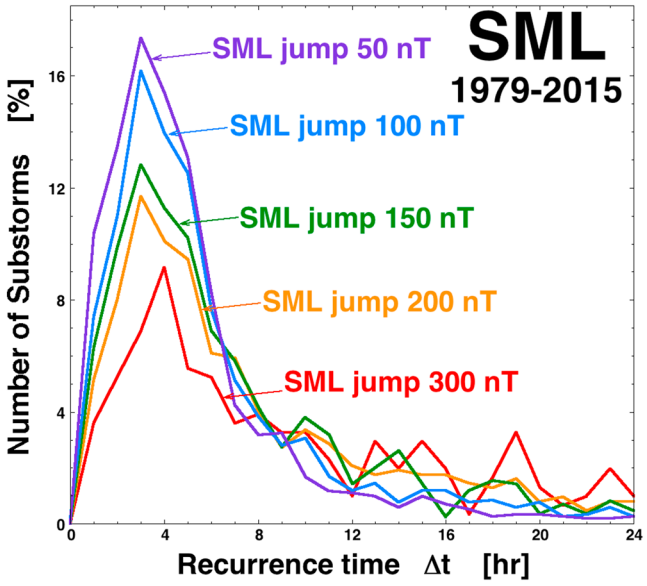

Figure 13. The recurrence-time distribution is plotted for SML-jump events in 1979–2015 is plotted for various amplitudes taken for the selection of events. The curves range from very small-amplitude events (purple) to large amplitude events (red). The distributions are all normalized such that the area under each curve is the same.

In Figure 13 the substorm recurrence-time distribution is examined for substorms of various amplitudes as measured by the magnitude of the jump in the SML index. In section 2 the substorm-selection criteria for the SML index was chosen to be a jump of 150 nT in 15 min. If that criterion is increased to above 150 nT, fewer events are selected, with only larger-amplitude events chosen. Similarly, if the criterion is lowered below 150 nT more events are chosen and the increase is in smaller events. In Figure 13 the recurrence-time distributions are plotted for various choices of the SML-jump criterion; the various curves in Figure 13 are normalized so that the area under each curve is the same. The red curve is the distribution for a 300 nT selection criterion and represents the recurrence-time distribution of larger-amplitude substorms. The yellow curve is the distribution when the criterion is 200 nT: this distribution contains the large-amplitude substorms in the 300 nT red curve plus substorms of more-modest amplitude. Likewise, the green distribution contains the orange distribution below it, which contains the red distribution. Note in Figure 13 that the location in Δt of the distribution of periodically occurring substorms does not shift as substorms of differing amplitudes are systematically added to the collection of substorms. This is an indication that the period of substorm recurrence is invariant to the amplitude of the substorms, a conclusion also reached by *Belian et al.* [1994].

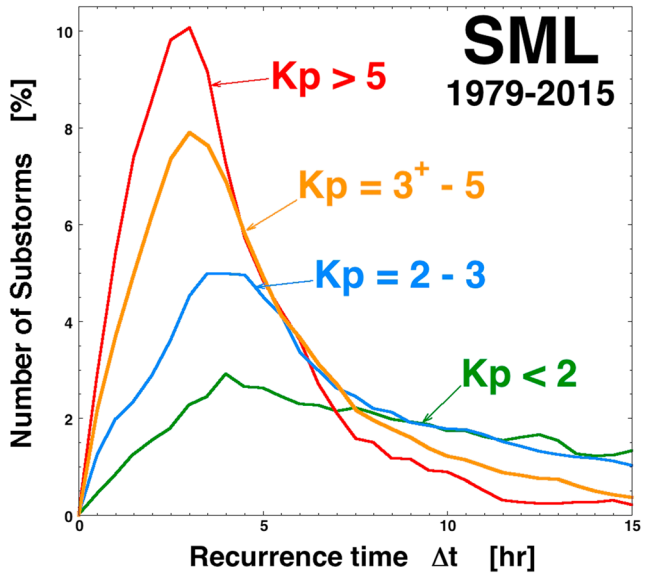

Figure 14. For 36 years, the recurrence-time distribution for substorms determined from jumps in the SML index is plotted separately for intervals of time when the *Kp* index was in various ranges as labeled.

To examine the recurrence period of the periodic population of substorms versus the level of geomagnetic activity, the *Kp* index is used, with *Kp* being a good measure of the strength of convection in the magnetosphere [*Thomsen*, 2004]. Figure 14 displays the substorm recurrence-time distribution for various levels of geomagnetic activity, plotting the distributions for four ranges of the *Kp* index. At very low *Kp* ($Kp < 2$, green curve) the population of periodic substorms is almost absent (i.e., periodically occurring substorms are rare when geomagnetic activity is very low). At a modest range of *Kp* levels ($2 \le Kp \le 3$; blue curve) the periodic population is weak but clearly present. (Note that the median value of *Kp* for all times is 2, which is in the range of the blue curve.) At

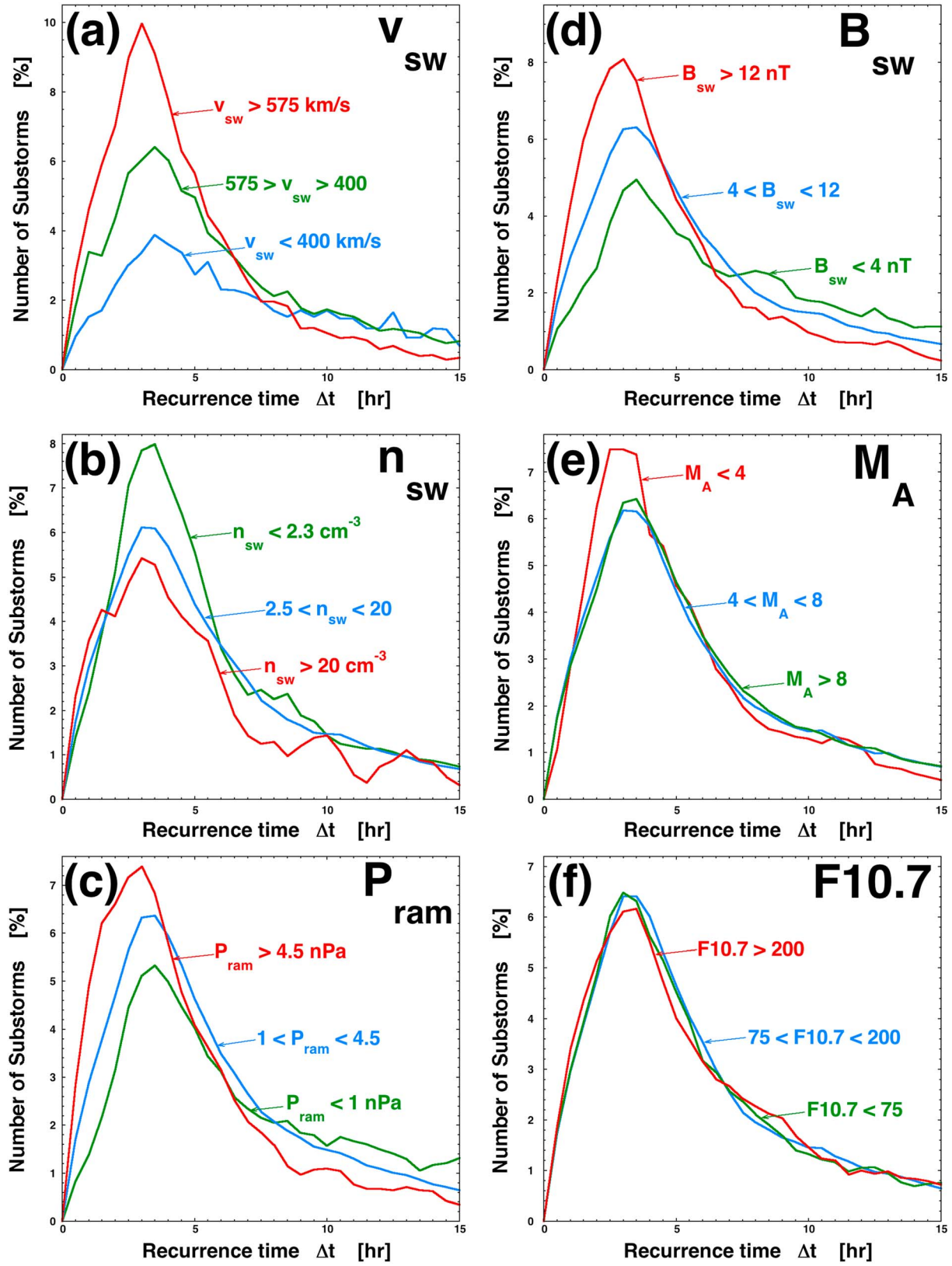

Figure 15. The recurrence-time distributions of substorms as determined from jumps in the SML index in 1979–1980 are plotted for various ranges of various solar and solar wind parameters. (a) The velocity v_{sw} of the solar wind. (b) The density n_{sw} of the solar wind. (c) The ram pressure P_{ram} of the solar wind. (d) The magnetic field strength B_{sw} in the solar wind. (e) The Alfven Mach number M_A of the solar wind. (f) The solar 10.7 cm radio flux $F_{10.7}$.

elevated levels of Kp ($3+ \leq Kp \leq 5$; orange curve) the periodic component dominates over the random component and periods in the range of 1.5–4.5 h are seen with a peak in the recurrence-time distribution at about $\Delta t = 3$ h. At high levels of Kp ($Kp > 5$; red curve) the periodic component is very dominant periods with in the range of 2–3.5 h seen with a peak in the recurrence-time distribution at about $\Delta t = 3$ h. No strong trend in the recurrence time of the periodic substorms is seen with geomagnetic activity as measured by the Kp index; however, there may be a weak trend toward shorter periods with increasing activity (comparing the orange and red curves). Note that a similar trend was not seen in Figure 13 when the period versus substorm amplitude was plotted.

Looking back at Figure 12, which displays the substorm-recurrence-time distributions in the four types of solar wind, it is seen that there is a slight shift toward shorter periods for the periodic population for ejecta (blue curve) relative to the other three types of plasma.

In the six panels of Figure 15 the substorm recurrence-time distribution is examined under various solar wind and solar conditions. All plots in Figure 15 pertain to substorms determined by jumps in the SML index. In Figures 15a and 15b the substorm recurrence times are plotted for various ranges of the solar wind velocity v_{sw} and for various ranges of the solar wind density n_{sw}; no strong variation of the period of recurrence is seen for variations in v_{sw} or n_{sw}. Figure 15c plots the substorm recurrence-time distribution for three ranges of the solar wind ram pressure P_{ram}; a trend is seen where the recurrence time of periodic substorms is lower when the ram pressure of the solar wind is very strong (red curve). The red curve distribution for very strong ram pressure exhibits recurrence times Δt of 1.5–4 h. In Figure 15d the substorm recurrence-time distributions are plotted for three ranges of the solar wind magnetic field strength $B_{sw} = |B_{sw}|$. A similar trend to that of P_{ram} in Figure 15c is seen, with the recurrence period of the periodic population being slightly lower for strong values of B_{sw} (red curve). In Figure 15c the substorm recurrence-time distributions are plotted for three ranges of the solar wind Alfven Mach number $M_A = v_{sw}/v_A \propto v_{sw} n_{sw}{}^{1/2}/B_{sw}$, where v_A is the Alfven speed in the solar wind upstream of the bow shock: a trend is seen where the period of substorm recurrence for the periodic population is slightly lower when the solar wind Mach number is low (red curve for $M_A < 4$). Low-Mach-number solar wind occurs almost exclusively when the solar wind type is ejecta [cf. *Lavraud and Borovsky*, 2008, Figure 1; *Xu and Borovsky*, 2015, Figure 16], and ejecta showed hints of a slightly reduced substorm-recurrence period in Figure 11. In Figure 15f the substorm recurrence-time distribution is plotted for three ranges of the solar $F_{10.7\,cm}$ flux values, with $F_{10.7}$ being a proxy for solar EUV flux. No systematic change in the substorm recurrence period of the periodic population is seen going from low values of solar $F_{10.7}$ (green curve) to high values of solar $F_{10.7}$ (red curve). Note that ionospheric ion composition, ionospheric ion outflows into the magnetosphere, and the ionic composition of the magnetosphere all vary with solar $F_{10.7}$ [e.g., *Lennartsson*, 1989; *Yau et al.*, 2011; *Welling et al.*, 2015]; this lack of change of the observed substorm period with solar $F_{10.7}$ may impact the hypothesis that ion outflow controls the periodicity of substorm occurrence [e.g., *Brambles*, 2011, 2013; *Ouellette et al.*, 2013].

In the two panels of Figure 16 the substorm recurrence-time distribution is plotted for three ranges of values of the *Siscoe et al.* [2004] polar-cap saturation parameter $Q = \Sigma_P v_A/796$ (cf. equation (22) of *Borovsky* [2013] physics) where Σ_P is the height-integrated Pedersen conductivity of the Earth's polar cap (in units of mhos) and v_A is the Alfven speed in the solar wind upstream of the Earth (in units of km/s). For an estimate of the Pedersen conductivity, the expression $\Sigma_P = 0.77\, F_{10.7}{}^{1/2}$ [*Ober et al.*, 2003] can be used, yielding $Q = F_{10.7}{}^{1/2} v_A/1034$. Note that $Q \propto F_{10.7}{}^{1/2} B_{sw}/n_{sw}{}^{1/2}$. The median value of Q is 0.56, and polar-cap potential saturation sets in as Q makes the transition from 1 to 2. In Figure 16 (top) the recurrence-time distributions of substorm onsets determined by jumps in the SML index are plotted for three ranges of the polar-cap potential saturation parameter: not saturated ($Q < 1$; green curve), in the transition to saturation ($1 \leq Q \leq 2$; blue curve), and saturated ($Q > 2$; red curve). A slight shift toward lower Δt values for the periodic substorms in the red curve is present compared with the other two curves. Figure 15f confirms this shift by repeating the analysis using the substorm onsets determined from electron injections. In both panels of Figure 15 the reduction of the average period of substorm recurrence is about 0.5 h for the $Q > 2$ distribution.

The reaction of the substorm-recurrence period to the various properties examined in this section is summarized in Table 4. The recurrence time of periodic substorms is reduced slightly for high values of Q, low values of M_A, and large values of B_{sw}: these three parameters are all associated with polar-cap potential saturation of the magnetosphere. The periodic-substorm recurrence time is reduced slightly in ejecta plasma relative to

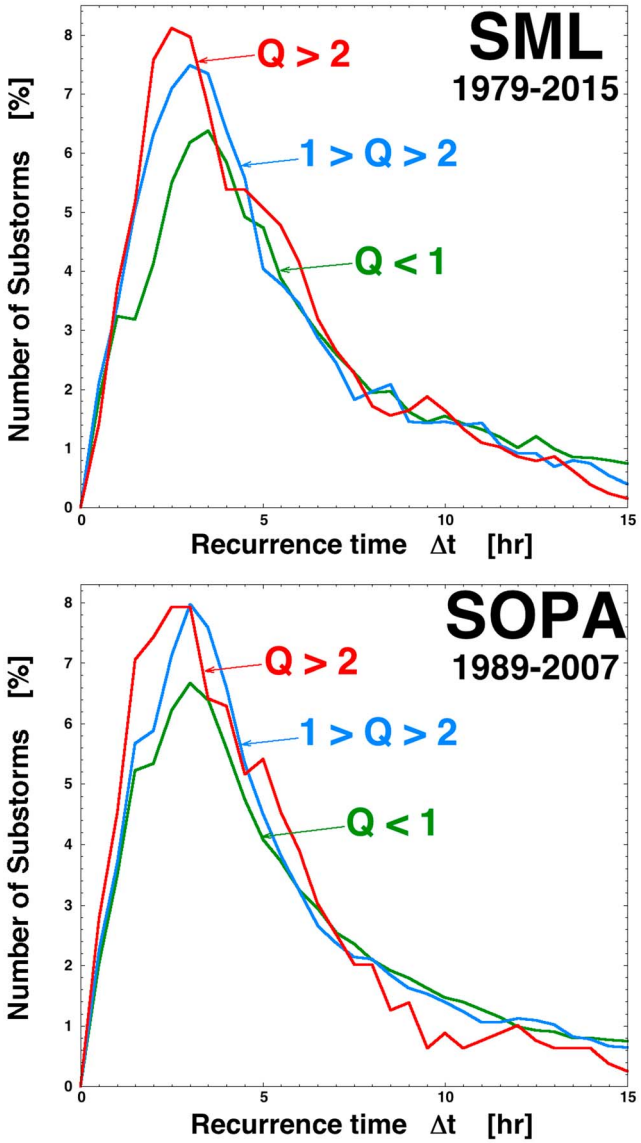

Figure 16. (top) For substorms as determined from jumps in the SML index in 1979–2015 and (bottom) for substorms as determined from electron injections in 1989–2007, the recurrence-time distribution is plotted separating the data into time intervals when the polar-cap-saturation parameter $Q = \Sigma_P v_A/796$ is in various ranges. The green curves represent times when the polar-cap potential is not saturated, the red curves represent times when the polar-cap potential is saturated, and the blue curves represent times when the potential is in transition toward saturation.

the other types of solar wind plasma. Note that global sawtooth oscillations are associated with low-Mach-number solar wind, with polar-cap potential saturation, and with magnetic clouds (a subset of ejecta plasma) [*Borovsky and Denton*, 2006; *Lavraud and Borovsky*, 2008]. The recurrence time of periodic substorms is also reduced slightly for high values of P_{ram} and high values of *Kp*. The recurrence period of periodic substorms does not appear to be affected by the amplitude of the substorms, by n_{sw}, *by* v_{sw}, nor by solar $F_{10.7}$.

7. Findings and Discussion

The findings of this study are the following:

1. Collections were made of 28,464 substorms identified with jumps in the SML index in the years 1979–2015 and 16,025 substorms identified with electron injections into geosynchronous orbit in the years 1989–2007.
2. The recurrence-time distributions of electron injection events and SML jumps have very similar properties.
3. The substorm recurrence-time distribution is composed of three populations: (a) quasiperiodic substorms with recurrence times of 2 to 4 h, (b) a population of randomly occurring substorms with recurrence times of about 6 to 15 h, and (c) long intervals of time (greater than about 24 h) wherein no substorms occur.
4. Substorm onsets are temporally associated with intervals of enhanced driving of the magnetosphere by the solar wind. This holds for both randomly occurring substorms and periodically occurring substorms.
5. Periodic substorms are associated with time intervals of stronger driving of the magnetosphere than are randomly occurring substorms.
6. The time scales of the variations of the magnetic field orientation of the solar wind do not control the ~3 h periodicity of substorm occurrence.
7. It is speculated that the substorm recurrence period may be associated with the combinations of (a) an inherent periodicity of the magnetosphere and (b) a solar wind time scale for producing an interval of driving sufficient for a substorm to occur.

Table 4. The Effects of Various Properties on the Recurrence Period of Periodic Substorms

Property	Quantity Examined	Effect on Recurrence Period Δt
Polar-cap potential saturation	Q	Period slightly less for high Q
Solar-wind Alfven Mach number	M_A	Period slightly less for low M_A
Solar-wind magnetic field strength	B_{sw}	Period slightly less for strong B_{sw}
Solar-wind ram pressure	P_{ram}	Period slightly less for high P_{ram}
Type of solar wind plasma		Period slightly less in ejecta plasma
Geomagnetic activity	Kp	Period slightly less for high Kp
Substorm amplitude	SML	Period independent of substorm amplitude
Solar-wind velocity	v_{sw}	Period independent of v_{sw}
Solar-wind density	n_{sw}	Period independent of n_{sw}
Solar EUV flux	$F_{10.7}$	Period independent of $F_{10.7}$

8. The occurrence statistics of the population of randomly occurring substorms are similar to (a) the occurrence statistics of changes in the clock angle of the solar wind magnetic field and (b) the occurrence statistics of solar wind driving intervals of above-average strength, both implying that randomly occurring substorms are associated with randomly occurring intervals of enhanced solar wind driving of the magnetosphere.
9. Substorm occurrence rates (number of substorms per day) are substantially higher during the declining phase of the solar cycle than they are during the other three phases of the solar cycle.
10. The additional substorms occurring during the declining phase are predominantly periodically occurring substorms.
11. Substorm occurrence is weaker in summer than it is in the other three seasons of the year, but not as weak as was found in prior studies.
12. There is a Russell-McPherron effect to the occurrence rate of substorms in spring and in fall that changes the occurrence rates by tens of percent depending on whether the Earth is in a toward or away solar wind magnetic sector.
13. Examining the type of solar wind plasma at Earth, substorm occurrence rates are highest in coronal-hole-origin plasma, weakest in sector-reversal-region plasma, and near average in both streamer-belt-origin plasma and ejecta plasma.
14. Much of the increase in substorm occurrence in coronal-hole-origin plasma is owed to an increase in the number of periodically occurring substorms. Periodically occurring substorms are prevalent in coronal-hole-origin plasma.
15. Periodic substorms are almost absent in sector-reversal-region plasma, and long intervals without the occurrence of substorms are prevalent.
16. The recurrence period of periodically occurring substorms is slightly shorter in ejecta plasma than it is in the other types of solar wind plasma.
17. The recurrence period of periodically occurring substorms does not depend on the amplitude of the substorms.
18. The recurrence period of periodically occurring substorms is slightly shorter when geomagnetic activity is very high.
19. The recurrence period of periodically occurring substorms is slightly shorter when (a) the ram pressure P_{ram} of the solar wind is high, (b) the magnetic field strength B_{sw} of the solar wind is strong, (c) the Mach number M_A of the solar wind is low, and (d) the polar-cap potential saturation parameter Q is high.
20. Several of the quantities that reduce (slightly) the recurrence period of periodically occurring substorms are connected with polar-cap potential saturation: Q, B_{sw}, M_A, and ejecta.
21. Several quantities do not affect the recurrence period of periodically occurring substorms: (a) the solar wind speed v_{sw}, (b) the solar wind density n_{sw}, and (c) the solar EUV flux as proxied by solar $F_{10.7}$.

7.1. A Working Picture of Substorm Occurrence Controlled by the Solar Wind

In this study a working picture is presented of substorms occurring in three populations (cf. Figure 2): (1) a population of periodically occurring substorms with recurrence periods of 2–4 h (green curve in Figure 2), (2) a population of randomly occurring substorms with recurrence time scales Δt in the range of about

6–15 h (red curve in Figure 2), and (3) a population of substorms occurring after long intervals wherein no substorms occurred (orange curve in Figure 2).

7.1.1. The Periodically Occurring Substorms

The onset of a periodic substorm is temporally associated with an interval of solar wind driving of the magnetosphere (blue curves in Figure 5), but no evidence was found for a recurrence time in solar wind magnetic field direction changes that might be responsible for the 2–4 h periodicity of substorm occurrence (Figure 6). Hence, it is suggested that the period of substorm recurrence is set by some properties of the magnetosphere-ionosphere system independent of solar wind driving, but that a substorm will not occur until an interval of enhanced solar wind driving occurs after the magnetosphere becomes ready for substorm occurrence. Hence, it is speculated that the period of recurrence is set by the magnetosphere, but that the actual time of occurrence varies because of the random intervals of solar wind driving needed to set up the magnetosphere for a substorm. This might be expressed as the recurrence time being $\Delta t = \Delta t_{\text{magnetosphere}} + \Delta t_{\text{driving}}$ where $\Delta t_{\text{magnetosphere}}$ is a fixed time (maybe ~2 h) and $\Delta t_{\text{driving}}$ is a random number that varies from 0.5 to 2 h. Note in Figure 4 that the solar wind driving (black curve) varies on a time scale faster than the recurrence time of periodic substorms (distances between the red points or between the blue points). Every recurrence interval Δt will vary in length owing to the random values of $\Delta t_{\text{driving}}$, turning a periodic process into a quasiperiodic process.

7.1.2. The Randomly Occurring Substorms

Under weak solar wind driving, substorm occurrence becomes nonperiodic with an exponential distribution of waiting times (expression (2)) consistent with random occurrence. The time scales Δt for substorm recurrence for this population are in the range of 6–15 h. It makes sense that the occurrences of these substorms are caused by clock-angle variations of the IMF that are favorable enough to drive the magnetosphere strongly (if the plasma properties of the solar wind can support strong driving) so that the magnetosphere can be energized into having a substorm. These clock-angle temporal variations are caused by the advection past the Earth of mesoscale spatial structure of the vector magnetic field of solar wind. The exponential distribution of substorm waiting times (Figure 2) is similar to the exponential distribution of waiting times for the solar wind magnetic field clock angle (Figure 7).

7.1.3. The Long Intervals Without Substorms

Long time intervals in which no substorms occur are caused by the advection of plasma past the Earth that is unfavorable for driving substorms: the solar wind velocity may be too slow, the solar wind magnetic field may be too weak, etc. These properties of the solar wind plasma are slowly varying as compared with rapid variations in the direction of the solar wind magnetic field. For instance the solar wind velocity v_{sw} has an autocorrelation time of 53 h (cf. Table 6 of *Borovsky* [2012]vel]), meaning that intervals of slow solar wind can last typically ~53 h at Earth. It was found that the substorm recurrence-time distribution in sector-reversal-region plasma was dominated by long times Δt between substorms (Figure 12); intervals of sector-reversal region plasma at Earth can last for days.

This suggested working picture is similar to the concept underlying the solar wind -driven "minimal substorm model" of *Freeman and Morley* [2004], which successfully reproduces the observed recurrence-time distribution of substorm onsets. The minimal substorm model assumes that the Earth's magnetosphere has an intrinsic substorm-recurrence period that is the period of substorm recurrence under steady driving by the solar wind (such as would occur during the passage of a magnetic cloud where the variations in the magnetic field direction are small). Under nonsteady driving, the recurrence times of substorm onsets in the model deviate from the intrinsic period of the magnetosphere and are governed by the temporal structure of the solar wind driving. When driving is sufficient quasiperiodic substorms result, and when driving is sparse randomly occurring substorms result. For the quasiperiodic substorms, most recurrence times are longer than the intrinsic magnetospheric period, but some are shorter. Using actual solar wind data as input, the model describes the quasiperiodic recurrence population and the randomly occurring population. The period of periodically recurring substorms being slightly shorter in ejecta plasma (i.e., where there can be steady driving by magnetic clouds) and during high *Kp* (where driving is plentiful) agrees with this concept.

7.2. The Period of Periodic Substorms

A few related quantities (high B_{sw}, high Q, low M_A, high Kp, and ejecta) were found to be associated with a slightly reduced recurrence time for the quasiperiodic substorms (cf. Table 4). If, as suggested in

section 7.1 [cf. *Freeman and Morley*, 2004], the period of substorm recurrence is determined by a combination of (1) an intrinsic magnetospheric period $\Delta t_{\text{magnetosphere}}$ plus (2) the need for wait for an interval $\Delta t_{\text{driving}}$ of solar wind driving, then the various quantities (high B_{sw}, high Q, low M_A, high Kp, and ejecta) could be affecting either $\Delta t_{\text{magnetosphere}}$ or $\Delta t_{\text{driving}}$.

Reducing the waiting time for driving intervals $\Delta t_{\text{driving}}$ to shorten the substorm recurrence period could be related to high Kp, where driving is plentiful, and could be related to ejecta plasma, where the driving is steady because of the low levels of vector magnetic field fluctuations [cf. *Xu and Borovsky*, 2015, Figure 14e], particularly for the magnetic-cloud subset of ejecta [*Klein and Burlaga*, 1982; *Lepping et al.*, 2005]).

Low-Mach-number solar wind (low M_A) and polar-cap potential saturation (high Q) are associated with morphological changes to the magnetosphere, and these morphology changes could alter the intrinsic periodicity $\Delta t_{\text{magnetosphere}}$ of the reaction of the magnetosphere to the solar wind. The morphology changes are the following. Low M_A results in a low-β magnetosheath with an altered flow pattern [*Spreiter et al.*, 1966; *Biernat et al.*, 2000] including large-scale flow jets that increase the velocity shear along the magnetopause [*Lavraud et al.*, 2007]. The anisotropic pressure of the low-β magnetosheath at low M_A results in a strongly distorted cross-sectional shape of the magnetosphere [*Lavraud and Borovsky*, 2008; *Lavraud et al.*, 2013]. Polar-cap potential saturation (high Q) results in (1) new current systems in the dayside magnetosphere [*Siscoe et al.*, 2004; *Lopez et al.*, 2008; *Borovsky et al.*, 2009], (2) changes in the connections and communications of current systems in the dayside magnetosphere [*Siscoe et al.*, 2002; *Lopez et al.*, 2008], (3) magnetic field strengths that are weaker than the dipole value in the dayside magnetosphere [*Hill et al.*, 1976; *Siscoe et al.*, 2004; *Borovsky et al.*, 2009], (4) magnetic field strengths that are stronger than the dipole value in the nightside magnetosphere [*Borovsky et al.*, 2009], (5) changes in the shape of the dayside magnetopause [*Raeder et al.*, 2001; *Merkin et al.*, 2005a, 2005b], (6) a sunward movement of the cusps [*Raeder et al.*, 2001; *Borovsky et al.*, 2009], (7) lobe pressure acting on the dayside dipole regions [*Ober et al.*, 2006; *Lavraud and Borovsky*, 2008], and (8) a buckling of dayside dipole magnetic field into a tail-like morphology [*Lavraud and Borovsky*, 2008; *Borovsky et al.*, 2009]. The weakening of the dayside magnetic field during polar cap saturation also leads to an earthward motion of the dayside magnetopause [*Borovsky et al.*, 2009], shrinking the spatial volume of the dayside magnetosphere. Another solar wind parameter that was found to be associated with shorter recurrence periods of substorms is high solar wind ram pressure P_{ram} (cf. Table 4): higher ram pressure also acts to decrease the volume of the magnetosphere [*Schield*, 1969; *Walker and Russell*, 1995].

Data analysis [*Shue and Kamide*, 2001], simulations [*Lopez et al.*, 2004], and theory [*Lavraud and Borovsky*, 2008] have demonstrated that at low Mach numbers geomagnetic activity is positively correlated with the number density of the solar wind. *Borovsky and Birn* [2014] derived a low-Mach-number solar wind driving function for the magnetosphere with the functional form $\sin^2(\theta_{\text{sw}}/2)\ n_{\text{sw}}{}^{0.24}\ v_{\text{sw}}{}^{1.49}\ B_{\text{sw}}{}^{0.51}$, where n_{sw}, v_{sw}, and B_{sw} are the density, velocity, and magnetic field strength of the solar wind and θ_{sw} is the magnetic clock angle of the solar wind. Changes in any one of these four solar wind variables will result in changes in the driving of the magnetosphere. This opens the possibility that in the absence of variations of other variables, the solar wind number density could control the timing of intervals of driving and hence control the occurrence of substorms.

7.3. Global Sawtooth Oscillations

Global sawtooth oscillations are a subcategory of periodic substorms wherein the magnetic field in the dayside magnetosphere undergoes stretching and dipolarization and dispersionless particle injections can be seen in the dayside: the strict definition of global sawtooth oscillations is that magnetic field dipolarization and dispersionless particle injections are seen sunward of the dawn and dusk terminators [*Borovsky*, 2004]. In a global sawtooth oscillation, a substorm-like dipolarization of the magnetic field can even occur at local noon. Typical substorms involve time-dependent current systems that are restricted to the nightside magnetosphere, whereas global sawtooth oscillations involve time-dependent current systems that form in the dayside magnetosphere. Global sawtooth oscillations are associated with low-Mach-number solar wind [*Borovsky*, 2004; *Borovsky and Denton*, 2006; *Pulkkinen et al.*, 2007; *Lavraud and Borovsky*, 2008; *DeJong et al.*, 2009; *Cai et al.*, 2011] and tend to occur during the passage of magnetic clouds [*Borovsky and Denton*, 2006; *Lavraud and Borovsky*, 2008], which are a subset of ejecta plasma. Global sawtooth oscillations are intimately related to polar-cap potential saturation [*Borovsky and Denton*, 2006; *Lavraud and Borovsky*,

2008; *Borovsky et al.*, 2009]; polar-cap potential saturation changes the nature of currents in the dayside magnetosphere [*Siscoe et al.*, 2004; *Lopez et al.*, 2008; *Siscoe*, 2011; *Borovsky et al.*, 2009] and changes the morphology of the dayside magnetic field [*Raeder et al.*, 2001; *Merkin et al.*, 2005a, 2005b; *Borovsky et al.*, 2009]. In the present study, global sawtooth oscillations were not separately identified from substorms. In examining the recurrence period of periodically occurring substorms in this study, it was noted that there was a slight decrease in the recurrence period for low Mach numbers (Figure 15e), for strong solar wind magnetic field (Figure 15d), for a large polar-cap-saturation Q parameter (Figure 16), and for ejecta plasma (Figure 12), all of which are characteristics of the times when global sawtooth oscillations have been identified. It may be that the recurrence period of global oscillations are statistically slightly less (by about 0.5 h) than the recurrence period of ordinary substorms. This reduction in period may be related to the strong driving of the magnetosphere: during times of strong driving the magnetosphere has only a short wait for a driving interval after the intrinsic time scale of the magnetosphere is up.

Acknowledgments

The authors thank Joachim Birn, Mick Denton, Alexandre Koustov, Bob McPherron, and Steve Morley for helpful conversations, and the authors thank Tom Cayton for the SOPA energetic-electron fits and Jesper Gjerloev for his help with the SML data. This work was supported at the Space Science Institute by the NASA Heliophysics LWS TRT program via grants NNX14AN90G and NNX16AB75G, by the NSF GEM program via award AGS-1502947, by the NSF Solar-Terrestrial program via grant AGS-1261659, and by the NASA Heliophysics Guest Investigator program via grant NNX14AC15G and at the University of Michigan by the NASA Geospace SR&T program via grant NNX12AD29G. K.Y. wishes to thank the Los Alamos National Laboratory for a Vela Fellowship. Substorm lists and event-selection algorithms are available upon request from Joe Borovsky at jborovsky@spacescience.org or from Kateryna Yakymenko at kateryna.yakymenko@usask.ca: the substorm event lists have been submitted as supporting information to this journal article.

References

Anderson, B. J., M. J. Engebretsson, S. P. Rounds, L. J. Zanetti, and T. A. Potemra (1990), A statistical study of Pc3-5 pulsations observed by the AMPTE/CCE Magnetic Field Experiment 1. Occurrence distribution, *J. Geophys. Res.*, *95*, 10,495–10,523, doi:10.1029/JA095iA07p10495.

Bame, S. J., J. R. Asbridge, W. C. Feldman, J. T. Gosling, and R. D. Zwickl (1981), Bi-directional streaming of solar wind electrons >80 eV: ISEE evidence for a closed-field structure within the drive gas of an interplanetary shock, *Geophys. Res. Lett.*, *8*, 173–176, doi:10.1029/GL008i002p00173.

Baumjohann, W., and Y. Kamide (1984), Hemispherical Joule heating and the AE indices, *J. Geophys. Res.*, *89*, 383–388, doi:10.1029/JA089iA01p00383.

Baumjohann, W., G. Paschmann, T. Nagai, and H. Luhr (1991), Superposed epoch analysis of the substorm plasma sheet, *J. Geophys. Res.*, *96*, 11,605–11,608, doi:10.1029/91JA00775.

Belian, R. D., J. E. Borovsky, R. J. Nemzek, and C. W. Smith (1994), Random and periodic substorms and their origins in the solar wind, *Proceedings of the Second International Conference on Substorms*, p. 463, Univ. of Alaska.

Belian, R. D., T. E. Cayton, and G. D. Reeves (1995), Quasi-periodic global substorm generated flux variations observed at geosynchronous orbit, in *Space Plasmas: Coupling Between Small and Medium Scale Processes, Geophys. Monogr. Ser.*, vol. 86, edited by M. Ashour-Abdalla, T. Chang, and P. Dusenbery, 143 pp., AGU, Washington, D. C.

Belian, R. D., T. E. Cayton, R. A. Christiansen, J. C. Ingraham, M. M. Meier, G. D. Reeves, and A. J. Lazarus (1996), Relativistic electrons in the outer-zone: An 11 year cycle; Their relation to the solar wind, in *AIP Proceedings 383 Workshop on the Earth's Trapped Particle Environment*, edited by G. D. Reeves, p. 13, Am. Inst. of Physics, Woodbury, New York.

Biernat, H. K., N. V. Erkaev, C. J. Farrugia, D. F. Bogl, and W. Schaffenberger (2000), MHD effects of the solar wind flow around planets, *Nonlinear Processes Geophys.*, *7*, 201, doi:10.5194/npg-7-201-2000.

Birn, J., M. F. Thomsen, J. E. Borovsky, G. D. Reeves, D. J. McComas, R. D. Belian, and M. Hesse (1998), Substorm electron injections: Geosynchronous observations and test particle simulations, *J. Geophys. Res.*, *103*, 9235–9248, doi:10.1029/97JA02635.

Birn, J., M. F. Thomsen, J. E. Borovsky, G. D. Reeves, and M. Hesse (2000), Particle acceleration in the dynamic magnetotail, *Phys. Plasmas*, *7*, 2149, doi:10.1063/1.874035.

Borovsky, J. E. (2004), Global sawtooth oscillations of the magnetosphere, *Eos Trans. AGU*, *85*(49), 525, doi:10.1029/2004EO490009.

Borovsky, J. E. (2008), The flux-tube texture of the solar wind: Strands of the magnetic carpet at 1 AU?, *J. Geophys. Res.*, *113*, A08110, doi:10.1029/2007JA012684.

Borovsky, J. E. (2010), On the variations of the solar-wind magnetic field about the Parker-spiral direction, *J. Geophys. Res.*, *115*, A09101, doi:10.1029/2009JA015040.

Borovsky, J. E. (2012), The velocity and magnetic-field fluctuations of the solar wind at 1 AU: Statistical analysis of Fourier spectra and correlations with plasma properties, *J. Geophys. Res.*, *117*, A05104, doi:10.1029/2011JA017499.

Borovsky, J. E. (2013), Physics based solar-wind driver functions for the magnetosphere: Combining the reconnection-coupled MHD generator with the viscous interaction, *J. Geophys. Res. Space Physics*, *118*, 7119–7150, doi:10.1002/jgra.50557.

Borovsky, J. E., and J. Birn (2014), The solar-wind electric field does not control the dayside reconnection rate, *J. Geophys. Res. Space Physics*, *119*, 751–760, doi:10.1002/2013JA019193.

Borovsky, J. E., and T. E. Cayton (2011), Entropy mapping of the outer electron radiation belt between the magnetotail and geosynchronous orbit, *J. Geophys. Res.*, *116*, A06216, doi:10.1029/2011JA016470.

Borovsky, J. E., and M. H. Denton (2006), The differences between CME-driven storms and CIR-driven storms, *J. Geophys. Res.*, *111*, A07S08, doi:10.1029/2005JA011447.

Borovsky, J. E., and R. J. Nemzek (1994), Substorm Statistics: Occurrences and amplitudes, *Proceedings of the Second International Conference on Substorms*, p. 93, Univ. of Alaska.

Borovsky, J. E., R. J. Nemzek, and R. D. Belian (1993), The occurrence rate of magnetospheric-substorm onsets: Random and periodic substorms, *J. Geophys. Res.*, *98*, 3807–3813, doi:10.1029/92JA02556.

Borovsky, J. E., B. Lavraud, and M. M. Kuznetsova (2009), Polar cap potential saturation, dayside reconnection, and changes to the magnetosphere, *J. Geophys. Res.*, *114*, A03224, doi:10.1029/2009JA014058.

Borovsky, J. E., D. T. Welling, M. F. Thomsen, and M. H. Denton (2014), Long-lived plasmaspheric drainage plumes: Where does the plasma come from?, *J. Geophys. Res. Space Physics*, *119*, 6496–6520, doi:10.1002/2014JA020228.

Borovsky, J. E., T. E. Cayton, M. H. Denton, R. D. Belian, R. A. Christensen, and J. C. Ingraham (2016), The proton and electron radiation belts at geosynchronous orbit: Statistics and behavior during high-speed-stream-driven storms, *J. Geophys. Res. Space Physics*, *121*, 5449–5488, doi:10.1002/2016JA022520.

Brambles, O. J., W. Lotko, B. Zhang, M. Wiltberger, J. Lyon, and R. J. Strangeway (2011), Magnetosphere sawtooth oscillations induced by ionospheric outflow, *Science*, *332*, 1183, doi:10.1126/science.1202869.

Brambles, O. J., W. Lotko, B. Zhang, J. Ouellette, J. Lyon, and M. Wiltberger (2013), The effects of ionospheric outflow on ICME and SIR driven sawtooth events, *J. Geophys. Res. Space Physics*, *118*, 6026–6041, doi:10.1002/jgra.50522.

Caan, M. N., R. L. McPherron, and C. T. Russell (1977), Characteristics of the association between interplanetary magnetic field and substorms, *J. Geophys. Res.*, *82*, 4837–4842, doi:10.1029/JA082i029p04837.

Caan, M. N., R. L. McPherron, and C. T. Russell (1978), The statistical magnetic signature of magnetospheric substorms, *Planet. Space Sci.*, *26*, 269, doi:10.1016/0032-0633(78)90092-2.

Cai, X., and C. R. Clauer (2009), Investigation of the period of sawtooth events, *J. Geophys. Res.*, *114*, A06201, doi:10.1029/2008JA013764.

Cai, X., M. G. Henderson, and C. R. Clauer (2006), A statistical study of magnetic dipolarization for sawtooth events and isolated substorms at geosynchronous orbit with GOES data, *Ann. Geophys.*, *24*(12), 3481.

Cai, X., J.-C. Zhang, C. R. Clauer, and M. W. Liemohn (2011), Relationship between sawtooth events and magnetic storms, *J. Geophys. Res.*, *116*, A07208, doi:10.1029/2010JA016310.

Cassak, P. A., and M. A. Shay (2007), Scaling of asymmetric magnetic reconnection: General theory and collisional simulations, *Phys. Plasmas*, *14*, 102114, doi:10.1063/1.2795630.

Cayton, T. E., and R. D. Belian (2007), Numerical modeling of the synchronous orbit particle analyzer (SOPA, Version 2) that flew on S/C 1990-095, LA Rep. LA-14335, Los Alamos Natl. Lab., Los Alamos, N. M.

Cayton, T. E., R. D. Belian, S. P. Gary, T. A. Fritz, and D. N. Baker (1989), Energetic electron components at geosynchronous orbit, *Geophys. Res. Lett.*, *16*, 147–150, doi:10.1029/GL016i002p00147.

Chu, X., R. L. McPherron, T.-S. Hsu, and V. Angelopoulos (2015), Solar cycle dependence of substorm occurrence and duration: Implications for onset, *J. Geophys. Res. Space Physics*, *120*, 2808–2818, doi:10.1002/2015JA021104.

Crooker, N. U., S. W. Kahler, D. E. Larson, and R. P. Lin (2004), Large-scale magnetic field inversions at sector boundaries, *J. Geophys. Res.*, *109*, A03108, doi:10.1029/2003JA010278.

Dai, L., J. R. Wygant, C. A. Cattell, S. Thaller, K. Derten, A. Beneman, X. Tang, R. H. Friedel, S. G. Claudpierre, and X. Tao (2014), Evidence for injection of relativistic electrons into the Earth's outer radiation belt via intense substorm electric fields, *Geophys. Res. Lett.*, *41*, 1133–1141, doi:10.1002/2014GL059228.

DeForest, S. E., and C. E. McIlwain (1971), Plasma clouds in the magnetosphere, *J. Geophys. Res.*, *76*, 3587–3611, doi:10.1029/JA076i016p03587.

DeJong, A. D., A. J. Ridley, X. Cai, and C. R. Clauer (2009), A statistical study of BRIs (SMCs), isolated substorms, and individual sawtooth injections, *J. Geophys. Res.*, *114*, A08215, doi:10.1029/2008JA013870.

Denton, M. H., J. E. Borovsky, and T. E. Cayton (2010), A density-temperature description of the outer electron radiation belt during geomagnetic storms, *J. Geophys. Res.*, *115*, A01208, doi:10.1029/2009JA014183.

Fairfield, D. H., and L. J. Cahill (1966), Transition region magnetic field and polar magnetic disturbances, *J. Geophys. Res.*, *71*, 155–169, doi:10.1029/JZ071i001p00155.

Fok, M.-C., T. E. Moore, and W. N. Spjeldvik (2001), Rapid enhancement of radiation belt electron fluxes due to substorm depolarization of the geomagnetic field, *J. Geophys. Res.*, *106*, 3873–3882, doi:10.1029/2000JA000150.

Forsyth, C., I. J. Rae, J. C. Coxon, M. P. Freeman, C. M. Jackman, J. Gjerloev, and A. N. Fazakerley (2015), A new technique for determining Substorm Onsets and Phases from Indices of the Electrojet (SOPHIE), *J. Geophys. Res. Space Physics*, *120*, 10,592–10,606, doi:10.1002/2015JA021343.

Freeman, M. P., and S. K. Morley (2004), A minimal substorm model that explains the observed statistical distribution of times between substorms, *Geophys. Res. Lett.*, *31*, L12807, doi:10.1029/2004GL019989.

Freeman, M. P., and S. K. Morley (2009), No evidence for externally triggered substorms based on superposed epoch analysis of IMF Bz, *Geophys. Res. Lett.*, *36*, L21101, doi:10.1029/2009GL040621.

Friedel, R. H. W., G. D. Reeves, and T. Obara (2002), Relativistic electron dynamics in the inner magnetosphere—A review, *J. Atmos. Sol. Terr. Phys.*, *64*, 265, doi:10.1016/S1364-6826(01)00088-8.

Gjerloev, J. W. (2012), The SuperMAG data processing technique, *J. Geophys. Res.*, *117*, A09213, doi:10.1029/2012JA017683.

Guo, J., T. I. Pulkkinen, E. I. Tanskanen, X. Feng, B. A. Emery, H. Liu, C. Liu, and D. Zhong (2014), Annual variations in westward auroral electrojet and substorm occurrence rate during solar cycle 23, *J. Geophys. Res. Space Physics*, *119*, 2061–2068, doi:10.1002/2013JA019742.

He, Z., H. Zhu, S. Liu, Q. Zong, Y. Wang, R. Lin, L. Shi, and J. Gong (2015), Correlated observations and simulations on the buildup of radiation belt electron fluxes driven by substorm injections and chorus waves, *Astrophys. Space Sci.*, *355*, 245.

Henderson, M. G. (2004), The May 2–3, 1986 CDAW-9C interval: A sawtooth event, *Geophys. Res. Lett.*, *31*, L11804, doi:10.1029/2004GL019941.

Henderson, M. G., G. D. Reeves, R. Skoug, M. F. Thomsen, M. H. Denton, S. B. Mende, T. J. Immel, P. C. Brandt, and H. J. Singer (2006a), Magnetospheric and auroral activity during the 18 April 2002 sawtooth event, *J. Geophys. Res.*, *111*, A01S90, doi:10.1029/2005JA011111.

Henderson, M. G., et al. (2006b), Substorms during the 10–11 August 2000 sawtooth event, *J. Geophys. Res.*, *111*, A06206, doi:10.1029/2005JA011111.

Hill, T. W., A. Dessler, and R. A. Wolf (1976), Mercury and Mars: The role of ionospheric conductivity in the acceleration of magnetospheric particles, *Geophys. Res. Lett.*, *3*, 429–432, doi:10.1029/GL003i008p00429.

Hones, E. W. (1977), Substorm processes in the magnetotail: Comments on 'On hot tenuous plasmas, fireballs, and boundary layers in the Earth's magnetotail', by L. A. Frank, K. L. Ackerson, and R. P. Lepping, *J. Geophys. Res.*, *82*, 5633–5643.

Hsu, T.-S., and R. L. McPherron (2002), An evaluation of the statistical significance of the association between northward turnings of the interplanetary magnetic field and substorm expansion onsets, *J. Geophys. Res.*, *107*(A11), 1398, doi:10.1029/2000JA000125.

Hsu, T.-S., and R. L. McPherron (2009), A statistical study of the spatial structure of interplanetary magnetic field substorm triggers and their associated magnetic response, *J. Geophys. Res.*, *114*, A02223, doi:10.1029/2008JA013439.

Hsu, T.-S., and R. L. McPherron (2012), A statistical analysis of substorm associated tail activity, *Adv. Space Res.*, *50*, 1317, doi:10.1016/j.asr.2012.06.034.

Huang, C.-S., G. D. Reeves, J. E. Borovsky, R. M. Skoug, Z. Y. Pu, and G. Le (2003a), Periodic magnetospheric substorms and their relationship with solar wind variations, *J. Geophys. Res.*, *108*(A6), 1255. doi:10.1029/2002JA009704.

Huang, C.-S., J. C. Foster, G. D. Reeves, G. Le, H. U. Frey, C. J. Pollock, and J.-M. Jahn (2003b), Periodic magnetospheric substorms: Multiple space-based and ground-based instrumental observations, *J. Geophys. Res.*, *108*(A11), 1411, doi:10.1029/2003JA009992.

Huang, C.-S., G. Lee, and G. D. Reeves (2004), Periodic magnetospheric substorms during fluctuation interplanetary magnetic field Bz, *Geophys. Res. Lett*, *31*, L14801, doi:10.1029/2004GL020180.

Huang, C.-S., G. D. Reeves, G. Le, and K. Yumoto (2005), Are sawtooth oscillations of energetic plasma particle fluxes caused by periodic substorms or driven by solar wind pressure enhancements?, *J. Geophys. Res.*, *110*, A07207, doi:10.1029/2004JD005101.

Ingraham, J. C., T. E. Cayton, R. D. Belian, R. A. Christensen, R. H. W. Friedel, M. M. Meier, G. D. Reeves, and M. Tuszewski (2001), Substorm injection of relativistic electrons to geosynchronous orbit during the great magnetic storm of March 24, 1991, *J. Geophys. Res.*, *106*, 25,759–25,776, doi:10.1029/2000JA000458.

International Telegraph, and Telephone Corporation (1979), Reference data for radio engineers, sect. 42-5, Howard Sams, Indianapolis.

Kahler, S., and R. P. Lin (1994), The determination of interplanetary magnetic field polarities around sector boundaries using E > 2 keV electrons, *Geophys. Res. Lett.*, *21*, 1575–1578, doi:10.1029/94GL01362.

Kamide, Y., and C. E. McIlwain (1974), The onset time of magnetospheric substorms determined from ground and synchronous satellite records, *J. Geophys. Res.*, *79*, 4787–4790, doi:10.1029/JA079i031p04787.

Kim, H.-J., A. A. Chan, R. A. Wolf, and J. Birn (2000), Can substorms produce relativistic outer belt electrons?, *J. Geophys. Res.*, *105*, 7721–7735, doi:10.1029/1999JA900465.

King, J. H., and N. E. Papitashvili (2005), Solar wind spatial scales in and comparisons of hourly Wind and ACE plasma and magnetic field data, *J. Geophys. Res.*, *110*, A02104, doi:10.1029/2004JA010649.

Klein, L. W., and L. F. Burlaga (1982), Interplanetary magnetic clouds at 1 AU, *J. Geophys. Res.*, *87*, 613–624, doi:10.1029/JA087iA02p00613.

Lavraud, B., and J. E. Borovsky (2008), Altered solar wind-magnetosphere interaction at low Mach numbers: Coronal mass ejections, *J. Geophys. Res.*, *113*, A00B08, doi:10.1029/2008JA013192.

Lavraud, B., J. E. Borovsky, A. J. Ridley, E. W. Pogue, M. F. Thomsen, H. Reme, A. N. Fazakerley, and E. A. Lucek (2007), Strong bulk plasma acceleration in Earth's magnetosheath: A magnetic slingshot effect?, *Geophys. Res. Lett.*, *34*, L14102, doi:10.1029/2007GL030024.

Lavraud, B., et al. (2013), Asymmetry of magnetosheath flows and magnetopause shape during low Alfven Mach number solar wind, *J. Geophys. Res. Space Physics*, *118*, 1089–1100, doi:10.1002/jgra.50145.

Lee, D.-Y., and K. W. Min (2002), Statistical features of substorm indicators during geomagnetic storms, *J. Geophys. Res.*, *107*(A11), 1371, doi:10.1029/2002JA009243.

Lennartsson, W. (1989), Energetic (0.1- to 16-keV/e) magnetospheric ion composition at different levels of solar F10.7, *J. Geophys. Res.*, *94*, 3600–3610, doi:10.1029/JA094iA04p03600.

Lepping, R. P., C.-C. Wu, and D. B. Berdichevsky (2005), Automatic identification of magnetic cloud-like regions at 1 AU: Occurrence rate and other properties, *Ann. Geophys.*, *23*, 2687, doi:10.5194/angeo-23-2687-2005.

Lezniak, T. W., R. L. Arnoldy, G. K. Parks, and J. R. Winkler (1968), Measurements and intensity of energetic electrons at the equator at 6.6 RE, *Radio Sci.*, *3*, 710–714.

Lopez, R. E., and T. von Rosenvinge (1993), A statistical relationship between the geosynchronous magnetic field and substorm electrojet magnitude, *J. Geophys. Res.*, *98*, 3851–3857, doi:10.1029/92JA01660.

Lopez, R. E., M. Wiltberger, S. Hernandez, and J. G. Lyon (2004), Solar wind density control of energy transfer to the magnetosphere, *Geophys. Res. Let.*, *31*, L08804, doi:10.1029/2003GL018780.

Lopez, R. E., S. Hernandez, K. Hallman, R. Valenzuela, J. Seiler, P. C. Anderson, and M. R. Hairston (2008), Field-aligned currents in the polar cap during saturation of the polar cap potential, *J. Atmos. Sol. Terr. Phys.*, *70*, 555, doi:10.1016/j.jastp.2007.08.072.

Lyons, L. R., G. T. Blanchard, J. C. Samson, R. P. Lepping, T. Yamamoto, and T. Moretto (1997), Coordinated observations demonstrating external substorm triggering, *J. Geophys. Res.*, *102*, 27,039–27,051, doi:10.1029/97JA02639.

McAllister, A. H., M. Dryer, P. McIntosh, H. Singer, and L. Weiss (1996), A large polar crown coronal mass ejection and a "problem" geomagnetic storms: April 14–23, 1994, *J. Geophys. Res.*, *101*, 13,497–13,515, doi:10.1029/96JA00510.

McDiarmid, I. B., and J. R. Burrows (1965), On an electron source fore the outer Van Allen radiation zone, *Can. J. Phys.*, *43*, 1161, doi:10.1139/p65-113.

McPherron, R. L., C. T. Russell, and M. P. Aubry (1973), Satellite studies of magnetospheric substorms on August 15, 1968 9. Phenomenological model for substorms, *J. Geophys. Res.*, *78*, 3131–3149.

McPherron, R. L., T. Terasawa, and A. Nishida (1986), Solar wind triggering of substorm expansion onset, *J. Geomag. Geoelectr.*, *38*, 1089, doi:10.5636/jgg.38.1089.

Meredith, N. P., R. B. Horne, and R. R. Anderson (2001), Substorm dependence of chorus amplitudes: Implications for the acceleration of electrons to relativistic energies, *J. Geophys. Res.*, *106*, 13,165–13,178.

Merkin, V. G., A. S. Sharma, K. Papadopoulos, G. Milikh, J. Lyon, and C. Goodrich (2005a), Global MHD simulations of the strongly driven magnetosphere: Modeling of the transpolar potential saturation, *J. Geophys. Res.*, *110*, A09203, doi:10.1029/2004JA010993.

Merkin, V. G., A. S. Sharma, K. Papadopoulos, G. Milikh, J. Lyon, and C. Goodrich (2005b), Relationship between the ionospheric conductance, field aligned current, and magnetopause geometry: Global MHD simulations, *Planet. Space Sci.*, *53*, 873, doi:10.1016/j.pss.2005.04.001.

Morley, S. K., and M. P. Freeman (2007), On the association between northward turnings on the interplanetary magnetic field and substorm onsets, *Geophys. Res. Lett.*, *34*, L08104, doi:10.1029/2006GL028891.

Morley, S. K., and M. G. Henderson (2010), Comment on "Investigation of the period of sawtooth events" by X. Cai and C. R. Clauer, *J. Geophys. Res.*, *115*, A02216, doi:10.1029/2009JA014721.

Nevanlinna, H., and T. I. Pulkkinen (1998), Solar cycle correlations of substorm and auroral occurrence frequency, *Geophys. Res. Lett.*, *25*, 3087–3090, doi:10.1029/98GL02335.

Newell, P. T., and J. W. Gjerloev (2011), Evaluation of SuperMAG auroral electrojet indices as indicators of substorms and auroral power, *J. Geophys. Res.*, *116*, A12211, doi:10.1029/2011JA016779.

Newell, P. T., and K. Liou (2011), Solar wind driving and substorm triggering, *J. Geophys. Res.*, *116*, A03229, doi:10.1029/2010JA016139.

Newell, P. T., T. Sotirelis, K. Liou, C.-I. Meng, and F. J. Rich (2007), A nearly universal solar wind-magnetosphere coupling function inferred from 10 magnetospheric state variables, *J. Geophys. Res.*, *112*, A01206, doi:10.1029/2006JA012015.

Noah, M. A., and W. J. Burke (2013), Sawtooth-substorm connections: A closer look, *J. Geophys. Res. Space Physics*, *118*, 5136–5148, doi:10.1002/jgra.50440.

Ober, D. M., N. C. Maynard, and W. J. Burke (2003), Testing the Hill model of transpolar potential saturation, *J. Geophys. Res.*, *108*(A12), 1467, doi:10.1029/2003JA010154.

Ober, D. M., N. C. Maynard, W. J. Burke, G. R. Wilson, and K. D. Siebert (2006), "Shoulders" on the high-latitude magnetopause: Polar/GOES observations, *J. Geophys. Res.*, *111*, A10213, doi:10.1029/2006JA011799.

Ouellette, J. E., O. J. Brambles, J. G. Lyon, W. Lotko, and B. N. Rogers (2013), Properties of outflow-driven sawtooth substorms, *J. Geophys. Res. Space Physics*, *118*, 3223–3232, doi:10.1002/jgra.50309.

Partamies, N., T. I. Pulkkinen, R. L. McPherron, K. McWilliams, C. R. Bryant, E. Tanskanen, H. J. Singer, G. D. Reeves, and M. F. Thomsen (2009), Statistical survey on sawtooth events, SMCs and isolated substorms, *Adv. Space Res.*, *44*, 376, doi:10.1016/j.asr.2009.03.013.

Prichard, D., J. E. Borovsky, P. M. Lemons, and C. P. Price (1996), Time dependence of substorm recurrence: An information-theoretic analysis, *J. Geophys. Res.*, *101*, 15,359–15,369, doi:10.1029/95JA03419.

Pulkkinen, T. I., N. Partamies, R. L. McPherron, M. Henderson, G. D. Reeves, M. F. Thomsen, and H. J. Singer (2007), Comparative statistical analysis of storm time activations and sawtooth events, *J. Geophys. Res.*, *112*, A01205, doi:10.1029/2006JA012024.
Raeder, J., Y. L. Wang, T. J. Fuller-Rowell, and H. J. Singer (2001), Global simulation of magnetospheric space weather effects of the Bastille day storm, *Sol. Phys.*, *204*, 325, doi:10.1023/A:1014228230714.
Rostoker, G. (1983), Triggering of expansive phase intensifications of magnetospheric substorms by northward turnings of the interplanetary magnetic field, *J. Geophys. Res.*, *88*, 6981–6993, doi:10.1029/JA088iA09p06981.
Russell, C. T., and R. L. McPherron (1973), Semiannual variation of geomagnetic activity, *J. Geophys. Res.*, *78*, 92–108, doi:10.1029/JA078i001p00092.
Sauvaud, J.-A., and J. R. Winckler (1980), Dynamics of plasma, energetic particles, and fields near synchronous orbit in the nighttime sector during magnetospheric substorms, *J. Geophys. Res.*, *85*, 2043–2056, doi:10.1029/JA085iA05p02043.
Schield, M. A. (1969), Pressure balance between solar wind and magnetosphere, *J. Geophys. Res.*, *74*, 1275–1286, doi:10.1029/JA074i005p01275.
Semenov, V. S., D. I. Kubyshkina, M. V. Kubyshkina, I. V. Kubyshkin, and N. Partamies (2015), On the correlation between the fast solar wind flow changes and substorm occurrence, *Geophys. Res. Lett.*, *42*, 5117–5124, doi:10.1002/2015GL064806.
Shue, J.-H., and Y. Kamide (2001), Effects of solar wind density on auroral electrojets, *Geophys. Res. Lett.*, *28*, 2181–2184, doi:10.1029/2000GL012858.
Siscoe, G., J. Rader, and A. J. Ridley, Transpolar potential saturation models compared (2004), *J. Geophys. Res.*, *109*, A09203, doi:10.1029/2003JA010318.
Siscoe, G. L. (2011), Aspects of global coherence of magnetospheric behavior, *J. Atmos. Sol. Terr. Phys.*, *73*, 402, doi:10.1016/j.jastp.2010.11.005.
Siscoe, G. L., N. U. Crooker, and K. D. Siebert (2002), Transpolar potential saturation: Roles of the region 1 current system and solar wind ram pressure, *J. Geophys. Res.*, *107*(A10), 1321, doi:10.1029/2001JA009176.
Smith, C. W., N. A. Schwadron, and C. E. DeForest (2013), Decline and recovery of the interplanetary magnetic field during the protracted solar minimum, *Astrophys. J.*, *775*, 59, doi:10.1088/0004-637X/775/1/59.
Southwood, D. J. (1976), A general approach to low-frequency instability in the ring current plasma, *J. Geophys. Res.*, *81*, 3340–3348, doi:10.1029/JA081i019p03340.
Spiro, R. W., M. Harel, R. A. Wolf, and P. H. Reiff (1981), Quantitative simulation of a magnetospheric substorm 3. Plasmaspheric electric fields and evolution of the plasmapause, *J. Geophys. Res.*, *86*, 2261–2272.
Spreiter, J. R., A. L. Summers, and A. Y. Alksne (1966), Hydromagnetic flow around the magnetosphere, *Planet. Space Sci.*, *14*, 223, doi:10.1016/0032-0633(66)90124-3.
Sreenivasan, K. R., A. Prabhu, and R. Narasimha (1983), Zero-crossings in turbulent signals, *J. Fluid Mech.*, *137*, 251, doi:10.1017/S0022112083002396.
Tanskanen, E., T. I. Pulkkinen, H. E. J. Koskinen, and J. A. Slavin (2002), Substorm energy budget during low and high solar activity: 1997 and 1999 compared, *J. Geophys. Res.*, *107*(A6), 1086, doi:10.1029/2001JA900153.
Tanskanen, E. I. (2009), A comprehensive high-throughput analysis of substorms observed by IMAGE magnetometer network: Years 1993–2003 examined, *J. Geophys. Res.*, *114*, A05204, doi:10.1029/2008JA013682.
Tanskanen, E. I., J. A. Slavin, A. J. Tanskanen, A. Viljanen, T. I. Pulkkinen, H. E. J. Koskinen, A. Pulkkinen, and J. Eastwood (2005), Magnetospheric substorms are strongly modulated by interplanetary high-speed streams, *Geophys. Res. Lett.*, *32*, L16104, doi:10.1029/2005GL023318.
Tanskanen, E. I., T. I. Pulkkinen, A. Viljanen, K. Mursula, N. Partamies, and J. A. Slavin (2011), From space weather toward space climate time scales: Substorm analysis from 1993 to 2008, *J. Geophys. Res.*, *116*, A00I34, doi:10.1029/2010JA015788.
Thomsen, M. F. (2004), Why Kp is such a good measure of magnetospheric convection, *Space Weather*, *2*, S11044, doi:10.1029/2004SW000089.
Walker, R. J., and C. T. Russell (1995), Solar-wind interactions with magnetized planets, in *Introduction to Space Physics*, edited by M. G. Kivelson and C. T. Russell, 164 pp., Cambridge Univ. Press, New York.
Welling, D. T., et al. (2015), The Earth: Plasma sources, losses, and transport processes, *Space Sci. Rev.*, *192*, 145, doi:10.1007/s11214-015-0187-2.
Weygand, J. M., R. L. McPherron, K. Kauristie, H. U. Frey, and T.-S. Hsu (2008), Relation of auroral substorm onset to local AL index and dispersionless particle injections, *J. Atmos. Sol. Terr. Phys.*, *70*, 2336, doi:10.1016/j.jastp.2008.09.030.
Wild, J. A., E. E. Woodfield, and S. K. Morley (2009), On the triggering of auroral substorms by northward turnings of the interplanetary magnetic field, *Ann. Geophys.*, *27*, 3559, doi:10.5194/angeo-27-3559-2009.
Xu, F., and J. E. Borovsky (2015), A new 4-plasma categorization scheme for the solar wind, *J. Geophys. Res. Space Physics*, *120*, 70–100, doi:10.1002/2014JA020412.
Yakymenko, K., and J. E. Borovsky (2016), Substorm occurrence rates as determined by various data sets, in *2016 Los Alamos Space Weather Summer School Research Reports*, p. 63, Report LA-UR-16-29471, Los Alamos Natl. Lab., Los Alamos, N. M.
Yau, A. W., W. K. Peterson, and T. Abe (2011), Influences of the ionosphere, thermosphere and magnetosphere on ion outflows, in *The Dynamic Magnetosphere*, edited by W. Liu and M. Fujimoto, p. 283, Springer Science+Business Media.
Yeoman, T. K., M. P. Freeman, G. D. Reeves, M. Lester, and D. Orr (1994), A comparison of midlatitude Pi 2 pulsations and geostationary orbit particle injections as substorm indicators, *J. Geophys. Res.*, *99*, 4085–4093, doi:10.1029/93JA03233.
Ylvisaker, N. D. (1965), The expected number of zeros of a stationary Gaussian process, *Ann. Math. Stat.*, *36*, 1043–1046, doi:10.1214/aoms/1177700077.
Zerbo, J.-L., and J. D. Richardson (2015), The solar wind during current and past solar minima and maxima, *J. Geophys. Res. Space Physics*, *120*, 10,250–10,256, doi:10.1002/2015JA021407.
Zolotukhina, N. A., P. N. Mager, and D. Y. Klimushkin (2008), Pc5 waves generated by substorm injection: A case study, *Ann. Geophys.*, *26*, 2053, doi:10.5194/angeo-26-2053-2008.